Related Papers
Multi-Instrument Observation of the Ionospheric Irregularities and Disturbances during the 23–24...
Study of ionospheric variability during geomagnetic storms
The study of topside ionospheric irregularities during geomagnetic storms in 2015
Study of Ionospheric behaviour during the intense geomagnetic storms in 24 th solar cycle over dif...
View more

ARTICLE IN PRESS

Available online at www.sciencedirect.com

ScienceDirect

Advances in Space Research xxx (xxxx) xxx

ADVANCES IN SPACE RESEARCH (a COSPAR publication)

www.elsevier.com/locate/asr

Ground and Space-based response of the ionosphere during the geomagnetic storm of 02–06 November 2021 over the low-latitudes across different longitudes

Sharon Aol [a,*], Valence Habyarimana [a], Patrick Mungufeni [b], Stephan C. Buchert [c], John Bosco Habarulema [d,e]

[a] Mbarara University of Science and Technology, Department of Physics, Mbarara P. O. Box 1410, Uganda
[b] Muni University, Department of Physics, Arua P.O. Box 725, Uganda
[c] Swedish Institute of Space Physics, Uppsala, Sweden
[d] South African National Space Agency, Hospital Street, Hermanus P. O. Box 32, South Africa
[e] Rhodes University Makhanda, Department of Physics and Electronics, 6139, Eastern Cape, P. O. Box 6140, South Africa

Received 14 August 2023; received in revised form 21 November 2023; accepted 13 December 2023

Abstract

The strong geomagnetic storm of class G3 that occurred on 03 November 2021 (Dst min = −118 nT, Kp = 8) was the first of this class recorded during the ascending phase of solar cycle 25. In this study, we examined the response of the ionosphere during the geomagnetic storm period from 02–06 November 2021 using the Total Electron Content (TEC) observations from a chain of Global Navigation Satellite System (GNSS) receiver stations in five longitudinal sectors i.e, Asian, East-African, West-African, South-American, and Pacific-west sectors, in the low-latitudes and space-based Swarm satellite electron density, N_e and TEC measurements. The Rate of Change of TEC Index (ROTI) was derived from the ground and space based TEC measurements to examine the occurrence of ionospheric irregularities. The Rate of change of electron density index (RODI) was also derived from Swarm N_e measurements to identify the occurrence of ionospheric irregularities at Swarm altitudes. A positive ionospheric storm effect was observed in all the longitudinal sectors considered in this study. A clear hemispherical asymmetry, with higher VTEC in the northern hemisphere was observed. The determining factors for ionospheric responses to this storm are; local time of the storm's onset, local time of storm's minimum SYM-H, and changes in thermospheric O/N_2 ratio. These geomagnetic storm effects were discussed in terms of the Prompt Penetration Electric Field (PPEF) storm induced wind lifting effect and Disturbance Dynamo Electric Field (DDEF). The geomagnetic storm inhibited the occurrence of ionospheric irregularities in all the sectors, during the main phase, except for three IGS receiver stations in South American sector. Overall, a longitudinal dependence of the enhancement/inhibition of ionospheric irregularities was observed. The generation of post-sunset irregularities was attributed to the local time occurrence of maximum ring current, PPEF and DDEF.
© 2023 Published by Elsevier B.V. on behalf of COSPAR.

Keywords: Total Electron Content (TEC); Geomagnetic storms; Ionospheric irregularities

1. Introduction

The interaction of the Sun and Earth may have significant effects on the magnetosphere-ionosphere-thermo sphere system, causing geomagnetic storms and ionospheric disturbances (Gonzalez and Tsurutani, 1987;

* Corresponding author.
E-mail address: saol@must.ac.ug (S. Aol).

https://doi.org/10.1016/j.asr.2023.12.032
0273-1177/© 2023 Published by Elsevier B.V. on behalf of COSPAR.

Please cite this article as: S. Aol, V. Habyarimana, P. Mungufeni et al., Ground and Space-based response of the ionosphere during the geomagnetic storm of 02–06 November 2021 over the low-latitudes across different longitudes, Advances in Space Research, https://doi.org/10.1016/j.asr.2023.12.032

Gonzalez et al., 1994). Intense geomagnetic storms are caused by Coronal Mass Ejections (CMEs) or High-Speed Streams (HSSs) (Lepping et al., 1991; Gonzalez et al., 1994; Gonzalez et al., 2001). Studying the variations in the ionosphere during geomagnetic storms is of great importance because they can significantly affect the performance of satellite communication and navigation systems (Buonsanto, 1999; Dashora et al., 2009; Srinivasu et al., 2019; Lissa et al., 2020). If the electron density of the ionosphere increases (decreases) as a result of storm dynamics, it is called a positive (negative) ionospheric storm (Prölss, 1995; Buonsanto, 1999). The complex disturbance traits of the ionosphere during geomagnetic storms are caused by different interacting atmospheric and electrodynamic processes, including but not limited to, the Prompt Penetration Electric Field (PPEF), Disturbance Dynamo Electric Field (DDEF), neutral winds, and subsequent compositional changes (Tsurutani et al., 2008; Klimenko and Klimenko, 2012).

Another important aspect of the ionospheric response to geomagnetic storms is the generation or inhibition of ionospheric irregularities. Typically, at equatorial/low latitudes, ionospheric irregularities are a night-time phenomenon and their occurrence is attributed to the generalized Rayleigh Taylor Instability (RTI) and the equatorial evening vertical plasma drift ($\vec{E} \times \vec{B}/B^2$) known as a pre-reversal enhancement (PRE) in vertical drift, when the eastward electric field is intensified due to the action of the F-region dynamo (Woodman and La-Hoz, 1976; Kil and Heelis, 1998; Fejer et al., 1999; Schunk and Nagy, 2009; Kelley, 2009). Depending on the phase of a geomagnetic storm, local time in a particular longitudinal sector, season or solar flux conditions, and type of the storm-induced electric fields causing upward/downward equatorial plasma drifts, this combination of factors can support or inhibit the formation of ionospheric irregularities. Disturbance electric fields i.e., PPEF and DDEF can penetrate the equatorial ionosphere and may support or inhibit the occurrence of ionospheric irregularities (Fejer, 1991). Attributed to the sudden southward turn of the interplanetary magnetic field z-component (IMF- Bz), the PPEFs are transmitted to the equator nearly instantly and have a short duration of $\sim 30-60$ min (Fejer and Scherliess, 1995; Kikuchi et al., 1996; Kikuchi et al., 2008; Tsurutani et al., 2008). However, long-lasting PPEFs (several hours) under the steady southward IMF-Bz have been reported (e.g, Huang et al., 2005). The PPEFs (under-shielding) are typically eastward in the daytime and westward at night-time, and being superimposed to the PRE can cause a much larger upward vertical drifts at the post-sunset sector (Fejer et al., 2008). In contrast, the DDEFs develop in $3-4$ hr after the storm initiation and are long-lived. The DDEFs are driven via global-scale thermospheric wind circulation due to Joule heating at high latitudes (Blanc and Richmond, 1980). The DDEFs are westward at daytime (downward drift) and eastward at nighttime (upward drift) and lead to a larger downward drift at the dusk (Richmond and Roble, 1997; Fejer et al., 2008). Thus, the occurrence of eastward DDEF near the local sunset period can support a strong upward plasma drift and generation of ionospheric irregularities over a narrow longitudinal sector. With storm development, long-lasting DDEFs dominate and support downward plasma drift near sunset thus promoting suppression of post-sunset ionospheric irregularities over a wide range of longitudes that can last for many hours or even days. Numerous studies have been done to understand ionospheric dynamics during geomagnetic storms at all latitudes (e.g, De Abreu et al., 2014; Ngwira et al., 2019; Zakharenkova et al., 2019; Aol et al., 2020b; Lissa et al., 2020; Younas et al., 2020; Astafyeva et al., 2020; Piersanti et al., 2020; Amaechi et al., 2021; Spogli et al., 2021; Palma et al., 2021; Imtiaz et al., 2021; Akala et al., 2021; Tang et al., 2022; Mansilla and Zossi, 2022; Cherniak and Zakharenkova, 2022). The geomagnetic storm which occurred during 02–06 November 2021 has been associated with three blending CMEs following solar flares according to a popularizing blog at `https://blogs.nasa.gov/solarcycle25/2021/11/`. The ionospheric effects of this storm have been the subject of several studies, among them are Wang et al. (2022),Wan et al. (2022), Regi et al. (2022),Zhai et al. (2022), Rukundo (2023),Oljira (2023). Wang et al. (2022) compared the atmospheric density data obtained by the polar orbiting spherical experimental of China satellite with the simulations of the Mass Spectrometer - Incoherent Scatter Model of the Upper Atmosphere (MSISE00) and the Drag Temperature Model (DTM). They found that the substantial disturbance enhancement and recovery of the atmospheric density of the dawn-dusk orbit have a close correlation with Kp and Dst indices. Wan et al. (2022) presented results concerning this geomagnetic storm and they restricted their study to the Pacific-America-Atlantic sector using European Space Agency's (ESAs) Swarm satellites, Defence Meteorological Satellite Program (DMSP), and Ionospheric Connection Explorer (ICON) satellite. They observed a persistent presence of strip-like bulges or electron density enhancement at lower-mid latitudes. Regi et al. (2022) examined the ionospheric response to this geomagnetic storm over the European and American sectors. They observed variations in the ionospheric parameters with negative and positive phases and reported longitudinal and latitudinal dependence of storm features in the European sector. From the results presented by Regi et al. (2022), the American sector analysis revealed negative storm signatures in electron concentration at the F2 region. Neutral composition and temperature changes were shown to be the main reason for the observed decrease in electron concentration in the American sector. Rukundo (2023) used daily variations of total electron content (TEC) from ground-based GNSS stations, ionosonde parameters and

Please cite this article as: S. Aol, V. Habyarimana, P. Mungufeni et al., Ground and Space-based response of the ionosphere during the geomagnetic storm of 02–06 November 2021 over the low-latitudes across different longitudes, Advances in Space Research, https://doi.org/10.1016/j.asr.2023.12.032

modeled zonal and meridional wind velocities to study the ionospheric response over the African region by comparing storm and quiet time variations. Oljira (2023) investigated the impact of this geomagnetic storm on TEC in a high-latitude auroral station at Tromso (Geog. Lat. +69.66°, Geog.Long. +18.94°, and Geomag.Lat. 66°) and a moderate occurrence of irregularity was observed during main and recovery storm phase at 18:00–24:00 UT and 1:00 UT-3:00 UT.

The ionospheric response to each storm is determined by a unique, complex, nonlinear, and even chaotic interaction of drivers playing their roles at a particular moment of time and in a particular location. This presents major difficulty in the analysis of storm-time effects and, consequently, in forecasting the ionospheric behavior during geomagnetic storms even by using most comprehensive first-principle models (Astafyeva et al., 2017; Borries et al., 2015). Furthermore, as stated by Akala et al. (2021), although earlier reports have detailed the sequence of events during geomagnetic storms, further observations are important as they can help to better understand such a complex phenomenon as the ionospheric storm. In this study, we complement the results reported about this geomagnetic storm, by highlighting the significant longitudinal differences of the response to the geomagnetic storm, particularly over the low- and mid- latitudes. An investigation conducted simultaneously at various longitudes under the same external conditions may yield significant information that is still pertinent and help us better understand the physical processes underlying the response of the ionosphere to geomagnetic storms at specific sectors (Bolaji et al., 2019). The rest of the paper is organized in the following order: The Data sources are presented in Section 2 and the Methods of Data analysis are presented in Section 3. The results are presented and discussed in Section 4. The summary and conclusions are presented in Section 5.

2. Data sources

To analyze the solar wind conditions during the geomagnetic storm period, solar wind parameters, at 1-min resolution were used and these included; the solar wind flow speed, IMF-Bz, and flow pressure P (Papitashvili and King, 2020). The geophysical conditions were represented by the geomagnetic perturbation indices: SYM-H and Kp indices. The solar wind and geophysical parameters are readily available at the Coordinated Data Analysis Web (CDAWeb) link (https://cdaweb.gsfc.nasa.gov).

For ground-based observations of the ionosphere, GPS-TEC from selected GPS receiver stations, installed over the low- and mid- latitudes, were used. The GPS data recorded in compact Receiver Independent Exchange (RINEX) format was downloaded from the University NAVSTAR Consortium (UNAVCO) website (`https://www.unavco.org`) and from the Crustal Dynamics Data Information System (CDDIS) website (`https://cddis.nasa.gov/index.html`). In addition, the geomagnetic storm-time ionospheric current variations were investigated using the quasi-definitive data obtained from magnetic observatories located in three selected longitudinal sectors. A total of 3 magnetometer stations were considered and the data of these magnetic observatories are available at `http://www.intermagnet.org`. The locations of the GPS receiver stations and magnetometer stations are presented in Fig. 1 as red dots and blue stars, respectively.

For Space-based measurements, the European Space Agency's (ESAs) Swarm satellites were used. The Swarm mission has three identical satellites (A, B, and C), each with payloads designed to measure the Earth's magnetic field and the space environment (Friis-Christensen et al., 2006). During the geomagnetic storm period, Swarm A and C orbited at an altitude of about 432 km in a near-polar orbit, while Swarm B orbited at an altitude of about 502 km above sea level. The Swarm orbital altitudes allow the study of processes that mainly occur in the topside F-region of the ionosphere. Each Swarm satellite carries upward-looking dual-frequency GPS receivers to enable Precise Orbit Determination (POD) with a position accuracy of a few centimeters and they can track up to eight GNSS satellites at 1 Hz (Buchert et al., 2015; Zakharenkova et al., 2019). The GPS L1-C/A and L2-P (Y) signals can be tracked (Buchert et al., 2015). Swarm satellites also measure local electron density N_e using Langmuir Probes (LP). In this study, we considered the Swarm LP N_e recorded at a frequency of 2-Hz, and the GPS-TEC measurements collected during the low-latitude crossings i.e, quasi-dipole latitudes between -40° and $+40^\circ$, for the geomagnetically disturbed days. The data sets measured by Swarm can be downloaded from `http://earth.esa.int/swarm` and these data sets are also readily available at the Virtual environments for Earth Scientists (VirES) for Swarm platform (`https://vires.services/`). The VirES platform provides both a graphical web interface and an Application Programming Interface (API) to access and visualize Swarm data and models (Smith et al., 2022).

3. Methods of data analysis

The processing of the ground-based GPS vertical TEC (VTEC) data was done using the GPS-TEC application software (Seemala and Valladares, 2011). Only satellites for which the elevation angle was $\geqslant 30^\circ$ were considered to minimize multi-path errors. The degree of VTEC disturbance during the period of study was estimated by the deviation from median VTEC ($VTEC_{median}$) using the Equation (Adewale et al., 2011):

$$\Delta VTEC = \frac{VTEC - VTEC_{median}}{VTEC_{median}}. \quad (1)$$

To determine $VTEC_{median}$, the quietest days identified from the international service of geomagnetic indices `http://isgi.unistra.fr/` for the month of November, 2021 were considered (10 quiet days: 11–14,1

Please cite this article as: S. Aol, V. Habyarimana, P. Mungufeni et al., Ground and Space-based response of the ionosphere during the geomagnetic storm of 02–06 November 2021 over the low-latitudes across different longitudes, Advances in Space Research, https://doi.org/10.1016/j.asr.2023.12.032

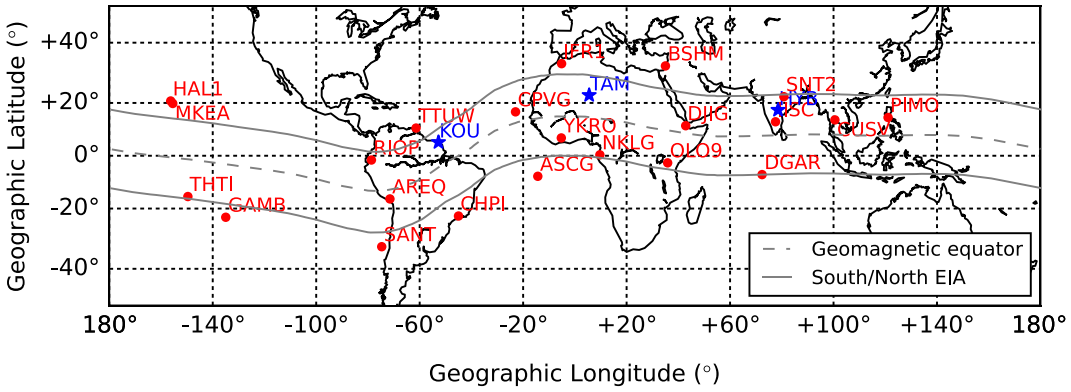


Fig. 1. World map showing the geographic location of IGS stations (red dots) and magnetometer stations (blue stars). The South and North EIA are represented by grey lines. The geomagnetic equator is represented by grey dashed line.

8–19,24–27 November 2021). The ΔVTEC was used to separate perturbation induced changes of TEC from regular behavior. A positive (negative) ΔVTEC is a signature of enhancement (depletion) in electron density. The small deviations in VTEC (±20%) were considered to be due to day-to-day variability in the ionosphere (Rishbeth, 1989) and could result due zonal wind effect or local gravity waves generated during thunderstorms or by local heating effects (Kumar et al., 2005). As these changes in VTEC may or may not have the effect of a geomagnetic storm, we do not discuss the small VTEC deviation in this paper. For Space-based VTEC observations, the signals transmitted by the GPS satellites are delayed by ionospheric or plasmaspheric electrons before reaching the Swarm GPS antenna (Laboratories, 2017). From the GPS signal delay, VTEC can be estimated (Noja et al., 2013). The Swarm VTEC product including the special mapping function for space-based receivers is described in SW-TR-GFZ-GS-0007 (available at `https://earth.esa.int/eogateway/catalog/swarm-level-2-daily`). The storm-related variation of the horizontal component H of the geomagnetic field was calculated using the Equation (Nava et al., 2016):

$$H = H_o + S_R + D_m + D_{iono}, \quad (2)$$

where H_o is the magnetic field produced in the Earth's core and crust, S_R represents the quiet daily variation of the geomagnetic field given as $S_q =< S_R >$, D_m is the disturbance related to the magnetospheric currents and D_{iono} is the magnetic field variations associated with the disturbed ionospheric currents. The D_m can be estimated by the following expression (Nava et al., 2016):

$$D_m = SYM - H \times \cos\phi, \quad (3)$$

where ϕ is the geomagnetic latitude, the SYMmetric Horizontal magnetic field (SYM-H) index is the estimation of the symmetric part of the ring current. Therefore, the final expression for D_{iono} becomes (Shimeis et al., 2012; Fathy et al., 2014; Azzouzi et al., 2015; Nava et al., 2016; Amory-Mazaudier et al., 2017; Akala et al., 2020):

$$D_{iono} = \Delta H - S_q - SYM - H \times \cos\phi \quad (4)$$

where ΔH is the variation of the H component of the Earth's magnetic field and can be obtained by subtracting H_o from the H component of the magnetic field (i.e $\Delta H = H - H_o$) (Vankadara et al., 2022). D_{iono} accounts for the combined effects of the disturbance polar No. 1 (DP1), the disturbance polar No.2 (DP2) which is the magnetic disturbance related to PPEF (Nishida, 1968), the disturbance polar No.3 (DP3), the disturbance polar No.4 (DP4), and ionospheric disturbed dynamo currents (D_{dyn}) which is related to DDEF (Blanc and Richmond, 1980), resulting from disturbance wind driven by auroral heating. At low/mid latitudes, the expression for day-side D_{iono} is given by (Le Huy and Amory-Mazaudier, 2005):

$$D_{iono} = DP2 + D_{dyn}. \quad (5)$$

Eq. 5 does not contain contribution from the polar disturbances DP1, DP3 and DP4 because the effect of these disturbances is ignorable on day-side low-to-mid latitude ionosphere (Amaechi et al., 2020). The storm-time variations in the H component and D_{iono} are computed from the data of individual stations.

To examine the occurrence of ionospheric irregularities from both ground-based and space-based GPS observations, the rate of change of TEC Index ROTI ($ROTI = \sqrt{\langle ROT^2 \rangle - \langle ROT \rangle^2}$) was used as a proxy (Pi et al., 1997; Basu et al., 1999; Oladipo et al., 2014; Amaechi et al., 2018). The ROT is the rate of change of TEC in TECU per minute. Overall, the ROT/ROTI is a rather simple and straightforward method which can be transferred to space-based GNSS measurements. The detailed description of this method implementation for the Swarm GNSS data is presented in Zakharenkova and Astafyeva (2015) and Zakharenkova and Cherniak (2018). In order to make the comparison between Space-based GPS and Swarm LP observations of ionospheric irregularities possible and more evident, the Swarm N_e data was processed in a similar way. Using the same approach as for the GPS data, Rate of change of density (ROD) in units of 10^6el(cm^3 min) and ROD index (RODI), based on the standard deviation of the ROD

$(\mathrm{RODI} = \sqrt{\langle \mathrm{ROD}^2 \rangle - \langle \mathrm{ROD} \rangle^2})$ was derived. The results are presented and discussed in the following section.

4. Results and discussions

4.1. The 02–06 November 2021 geomagnetic storm

The solar wind parameters and geomagnetic indices associated with this period are presented in Fig. 2. The figure presents variations of solar wind speed, IMF-Bz/IEF – Ey, proton pressure, P, SYM-H index and Kp index in panels (a)-(e), respectively as functions of Universal Time (UT). The instantaneous interplanetary electric field (IEF – Ey) (panel (b) [red]) from high latitude to low latitude is derived using the expression IEF – Ey = −solarwindspeed × IMF – Bz (Banks et al., 1984). A full-halo Coronal Mass Ejection (CME) left the Sun early on 02 November 2021, associated with an M-class solar flare (https://spaceweather.com/archive.php?view=1&day=02&month=11&year=2021, https://blogs.nasa.gov/solarcycle25/2021/11/). This CME affected the Earth's environment a few days later, starting late hours on 03 November 2021 and this caused the first strong geomagnetic storm of Solar Cycle 25. On 03 November 2021, the SYM-H instantly turned north at around 2000 UT and it rose to 50 nT at around 2100 UT on the same day, as observed in Fig. 2. The storm sudden commencement (SSC) started after 2100 UT on 03 November 2021 and the SYM-H decreased progressively reaching the minimum of −118 nT at about 1245 UT on 04 November 2021, under long-lasting southward conditions of the IMF-Bz, indicating the strong geomagnetic storm. Furthermore, the Kp index reached a maximum value of 8 at minimum SYM-H, while the solar wind speed rose to a peak value of about 800 km/s. The main phase lasted for about 15 h. The IEF – Ey was constantly eastward during the main phase of the storm with a magnitude of about 15 mV/m. The pressure showed a large increase during the period of southward directed IMF Bz and a maximum value of about 20 nPa was recorded. On 04 November 2021 after about 1245 UT, the recovery of the storm started and continued for a few days. During the recovery phase of the storm, the solar wind speed progressively decreased, indicating signatures of high speed solar wind and two peaks of about 630 km/s and 610 km/s, at around 1243 UT and 0135 UT were observed on 05 November 2021 and 06 November 2021, respectively. The IMF-Bz showed north and south fluctuations and with two positive peaks (above 5 nT) during recovery phase of the storm. The SYM-H variations during recovery phase showed two peaks coinciding with the peaks of the IMF-Bz and solar wind speed.

4.2. VTEC observations from the ground-based GNSS network during 02–06 November, 2021

The diurnal variations of ground-based VTEC during the geomagnetic storm period, at different longitude sectors are presented in Fig. 3 in panels (a) - (e). Each panel in

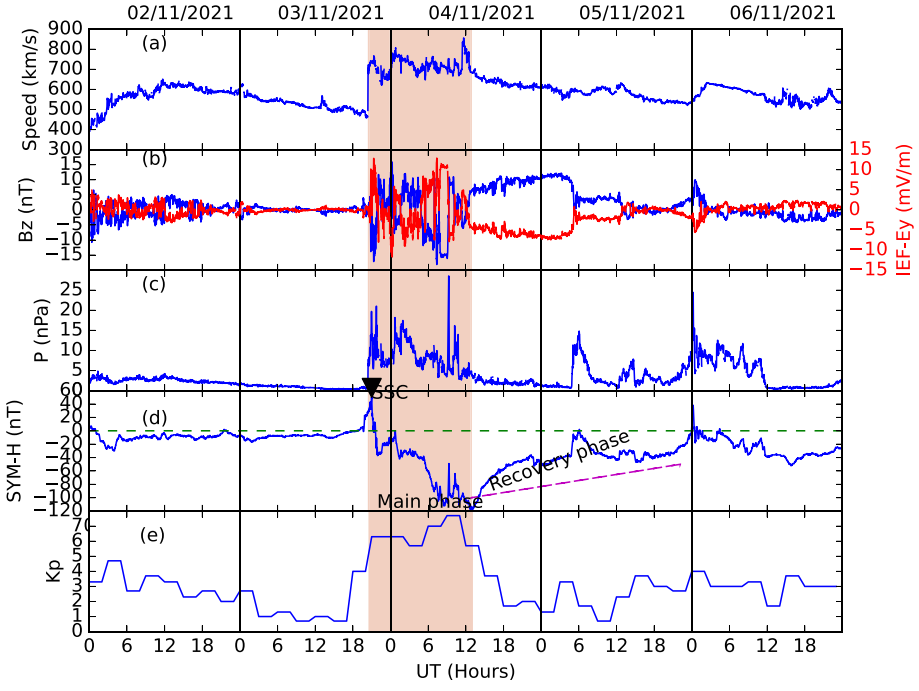


Fig. 2. The variation of (a) solar wind speed, (b) IMF-Bz/IEF-Ey, (c) pressure (P), (d) SYM-H index, and (e) Kp index during 02–06 November 2021. The SSC is indicated with a black arrow head. The pink region highlights the time range of the main phase of the geomagnetic storm.

Please cite this article as: S. Aol, V. Habyarimana, P. Mungufeni et al., Ground and Space-based response of the ionosphere during the geomagnetic storm of 02–06 November 2021 over the low-latitudes across different longitudes, Advances in Space Research, https://doi.org/10.1016/j.asr.2023.12.032

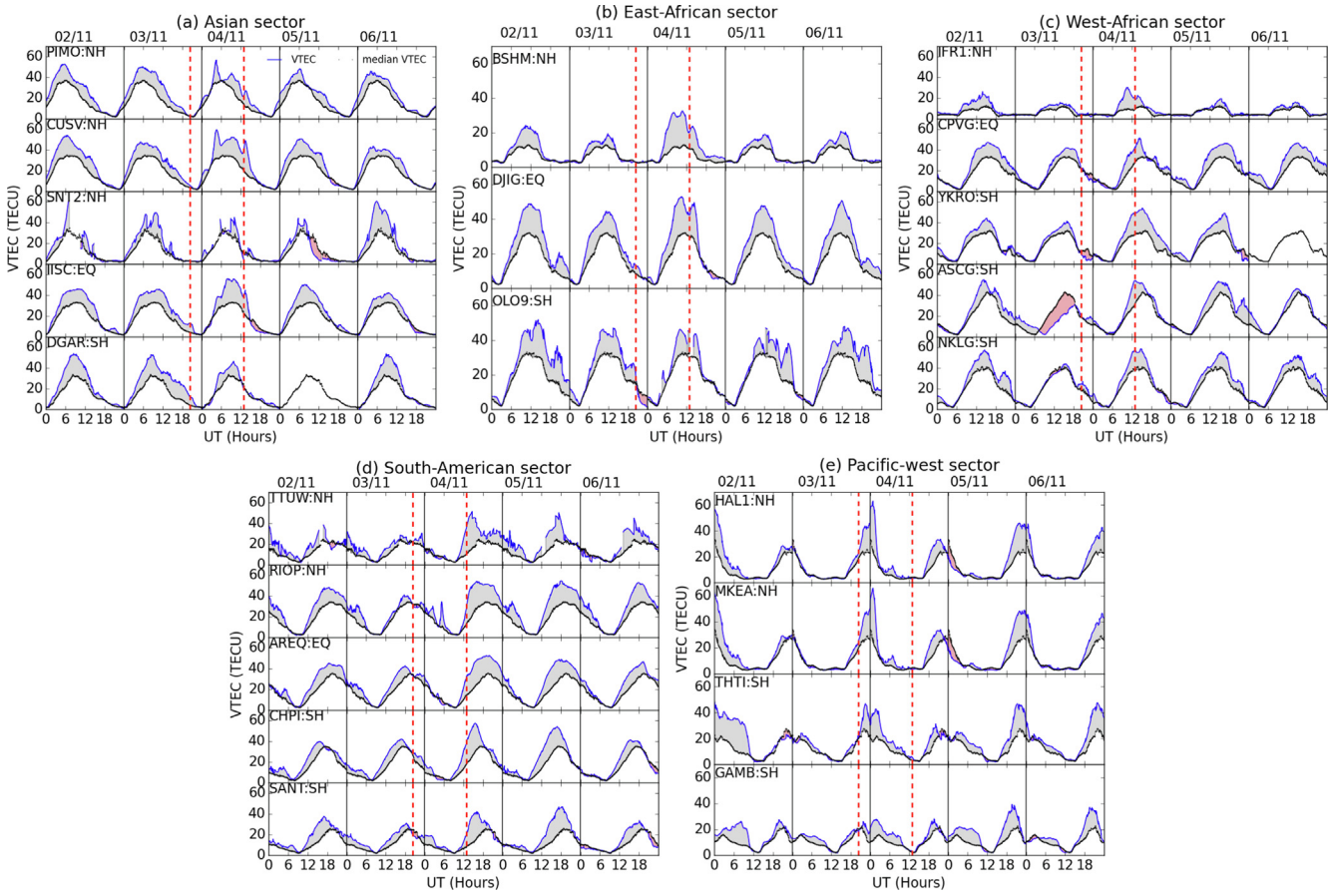


Fig. 3. Variation of VTEC (blue) and $VTEC_{median}$ (black) over GPS receiver stations installed in the different longitudinal sectors at low-latitudes during 02–06 November 2021, in panels (a) to (e). The two dotted vertical red lines show the duration of the main phase of the geomagnetic storm. The grey shaded regions represent a positive deviation of VTEC from $VTEC_{median}$, while the red shaded regions represent a negative deviation of VTEC from $VTEC_{median}$. Note. NH: Northern Hemisphere; SH: Southern Hemisphere; EQ: Magnetic Equator..

Fig. 3 also shows variation of quiet time VTEC ($VTEC_{median}$) as black dotted lines for comparison with VTEC during the geomagnetic storm period. The VTEC variations at different stations are arranged in decreasing order of geographic longitude from the East to the West (panels (a) - (e)). The normal diurnal pattern of VTEC shows a steady increase from about sunrise to an afternoon maximum just before sunset over all the GPS receiver stations. The peak of VTEC was seen to undergo a time shift from the East to the West. Therefore, the features of the geomagnetic storm development depend on the Local Time (LT) of a station (Sharma et al., 2011; Habarulema et al., 2013; Aol et al., 2020b). The storm's onset LT and the corresponding LT of the storm's minimum SYM-H are summarized in Table 1. The details of the IGS receiver stations and magnetometer stations are also summarized in Table 1. From Fig. 3, the VTEC values were observed to be higher during the main phase of the geomagnetic storm on 04 November, 2021, compared to the previous day on 03 November, 2021, except for DGAR and all the GPS receiver stations in the Pacific-west sector. In addition, generally, VTEC was higher than $VTEC_{median}$over all the GPS receiver stations in all longitudinal sectors during the main phase of the geomagnetic storm. The positive VTEC deviation over the stations may imply a positive ionospheric storm effect on 04 November 2021. Close inspection of Fig. 3 shows that, during the main phase of the geomagnetic storm on 04 November 2021, at the Asian sector, the highest VTEC values were recorded at CUSV and PIMO located near the North EIA, followed by IISC located near the geomagnetic equator and the least VTEC values were observed at DGAR which is located at the South EIA. It is important to note that there was a data gap in the VTEC values for SNT2 between 0000 UT and 0600 UT on 04 November 2021 and therefore, no conclusion was drawn for this station. At the East-African sector, during the main phase of the geomagnetic storm, the highest VTEC values were observed at DJIG located at the geomagnetic equator, followed by OLO9 located at the South EIA and the least was observed at BSHM located at the North EIA. In west African sector, the highest VTEC was observed at NKLG, and ASCG located at/near the South EIA, followed by YKRO and CPVG located closer to the geomagnetic equator and the least VTEC values were observed at IFR1 which is located near North EIA. At the East-South American sector, the highest VTEC

Please cite this article as: S. Aol, V. Habyarimana, P. Mungufeni et al., Ground and Space-based response of the ionosphere during the geomagnetic storm of 02–06 November 2021 over the low-latitudes across different longitudes, Advances in Space Research, https://doi.org/10.1016/j.asr.2023.12.032

value was recorded at CHPI located near the South EIA and the least VTEC was observed at TTUW located at the North EIA. At the West-South American sector, the highest VTEC was observed in RIOP at the North EIA followed by AREQ at the geomagnetic equator and the least at SANT located near the South EIA. At the Pacific-west sector, the highest VTEC value was recorded in HAL1 and MKEA located near the North EIA and the least was recorded in THTI and GAMB located in the South EIA. From Fig. 3, there is a clear hemispherical asymmetry. Similar observation was made by Akala et al. (2021) who examined longitudinal dependence of the ionospheric response to the geomagnetic storm of 26 August 2018 over the low-latitude region, where they reported hemispherical asymmetry to the advantage of the northern hemisphere at the expense of the southern hemisphere. The inter-hemisphere asymmetry has also been studied extensively at specific longitudinal sectors during different geomagnetic storms (e.g, Blagoveshchensky et al., 2003; Sahai et al., 2005; Huang and Yumoto, 2006; Astafyeva, 2009; De Abreu et al., 2010; Nava et al., 2016; Wan et al., 2022).

To quantify the level of VTEC increase (or decrease), the deviation ΔVTEC was derived for the ground-based IGS receivers and the results are presented in Fig. 4. The ΔVTEC represents the relative variation of VTEC on the disturbed days with respect to the quiet days. The positive (negative) ΔVTEC indicates a positive (negative) ionospheric storm effect on the geomagnetic storm day. In general, Fig. 4 shows that there was a moderate positive deviation in VTEC over stations in the Asian sector during the main phase of the geomagnetic storm on 04 November 2021. Over the East-African sector, during the main phase, a positive deviation was observed, with the highest ΔVTEC recorded at BSHM and the least at OLO9. Over the West-African sector (panel (c) Fig. 4), a positive deviation in VTEC was also observed during the main phase, with the highest ΔVTEC recorded at IFR1 and the least at NKLG. Over the South-American sector, ΔVTEC was positive at CHPI, RIOP, SANT, TTUW, and AREQ. The positive ionospheric storm over South America, on 4 November, 2021 was also reported by Zhai et al. (2022) based on multi-instrument observations from GNSS, DMSP, GOLD, ionosondes, SuperDARN, and ICON. Over the Pacific- west sector, positive ΔVTEC was observed for all the IGS receiver stations with the highest at MKEA and HAL1 and the least for THTI. Generally, all the six longitudinal sectors show positive storm effects. Similar observations were made by Younas et al. (2020) who presented the effects of the 25–29 August 2018 geomagnetic in several longitudinal sectors (Asia, Africa, America, and Pacific-west). The positive VTEC deviation over the stations implies a positive ionospheric storm effect on 04 November

Table 1
IGS and magnetometer stations used in this study. A summary of the local time (LT) zone from https://www.worldtimezone.com/, local time of minimum SYM-H. Note. NH: Northern Hemisphere; SH: Southern Hemisphere; EQ: Magnetic Equator.

IGS Station, country (Code:hemisphere or mag. Eq)	Geog. lat (°)	Geog. lon (°)	Mag. lat (°)	Lon. sector	LT(h)	LT of min. SYM-H
Quezon City, Metro Manila (PIMO:NH)	14.64	121.08	5.29	Asia	UT + 8	20:44
Patumwan, Bankok (CUSV:NH)	13.73	100.53	3.96	Asia	UT + 6	18:44
Sonatola, (SNT2:NH)	22.26	80.81	15.46	Asia	UT + 5	17:44
Bangalore, India (IISC:EQ)	13.02	77.57	4.61	Asia	UT + 5	17:44
Diego Garcia, India (DGAR:SH)	-7.27	72.37	-16.89	Asia	UT + 5	17:44
Haifa, Haifa District (BSHM:NH)	32.78	35.02	26.00	East-Africa	UT + 2	14:44
Observatoire Geophysique d'Arta, Djibouti (DJIG:EQ)	11.53	42.85	3.30	East-Africa	UT + 3	15:44
Engaresero, Tanzania (OLO9:SH)	−2.75	35.87	-12.37	East-Africa	UT + 3	15:44
IFRANE, Morocco (IFR1:NH)	33.51	−5.13	23.07	West-Africa	UT + 1	13:44
Libreville, Gabon (NKLG:SH)	0.35	9.67	-8.05	West-Africa	UT + 1	13:44
Yamoussoukro, Ivory coast (YKRO:SH)	6.87	−5.24	-2.60	West-Africa	UT	12:44
Ascension Island, Saint Helena (ASCG:SH)	−7.91	−14.33	-16.34	West-Africa	UT	12:44
Espargo, Cabo Verde. (CPVG:EQ)	16.73	−22.94	4.94	West-Africa	UT-1	11:44
Cachoeira Paulista, Brazil (CHPI:SH)	-22.69	−44.99	-14.21	South-America	UT-3	09:44
St. Augustine, Trinidad and Tobago (TTUW:NH)	10.64	−61.39	19.74	South-America	UT-4	08:44
Santiago, Chile (SANT:SH)	-33.15	-74.67	-19.52	South-America	UT-4	08:44
Ecuador, Riobamba (RIOP:NH)	-1.65	−78.65	10.56	South-America	UT-5	07:44
Arequipa, Peru (AREQ:EQ)	-16.47	-71.49	-3.79	South-America	UT-5	07:44
Haleakala, (HAL1:NH)	20.71	−156.25	21.30	Pacific-west	UT-10	02:44
Mauna Kea, USA (MKEA:NH)	19.80	−155.46	20.54	Pacific-west	UT-10	02:44
Papeete, French Polynesia (THTI:SH)	-15.58	−149.61	-13.18	Pacific-west	UT-10	02:44
Rikitea, French Polynesia (GAMB:SH)	-23.13	−134.97	-19.93	Pacific-west	UT-10	02:44
Magnetometer Station, country (Code)						
	Geog. lat (°)	Geog. lon (°)	Mag. lat (°)	Lon. sector		
Hyderabad, India (HYB)	17.42	78.55	9.06	Asia		
Tamanrasset, Algeria (TAM)	22.79	5.53	24.25	Africa		
French Guiana, (KOU)	5.21	-52.72	13.96	South-America		

Please cite this article as: S. Aol, V. Habyarimana, P. Mungufeni et al., Ground and Space-based response of the ionosphere during the geomagnetic storm of 02–06 November 2021 over the low-latitudes across different longitudes, Advances in Space Research, https://doi.org/10.1016/j.asr.2023.12.032

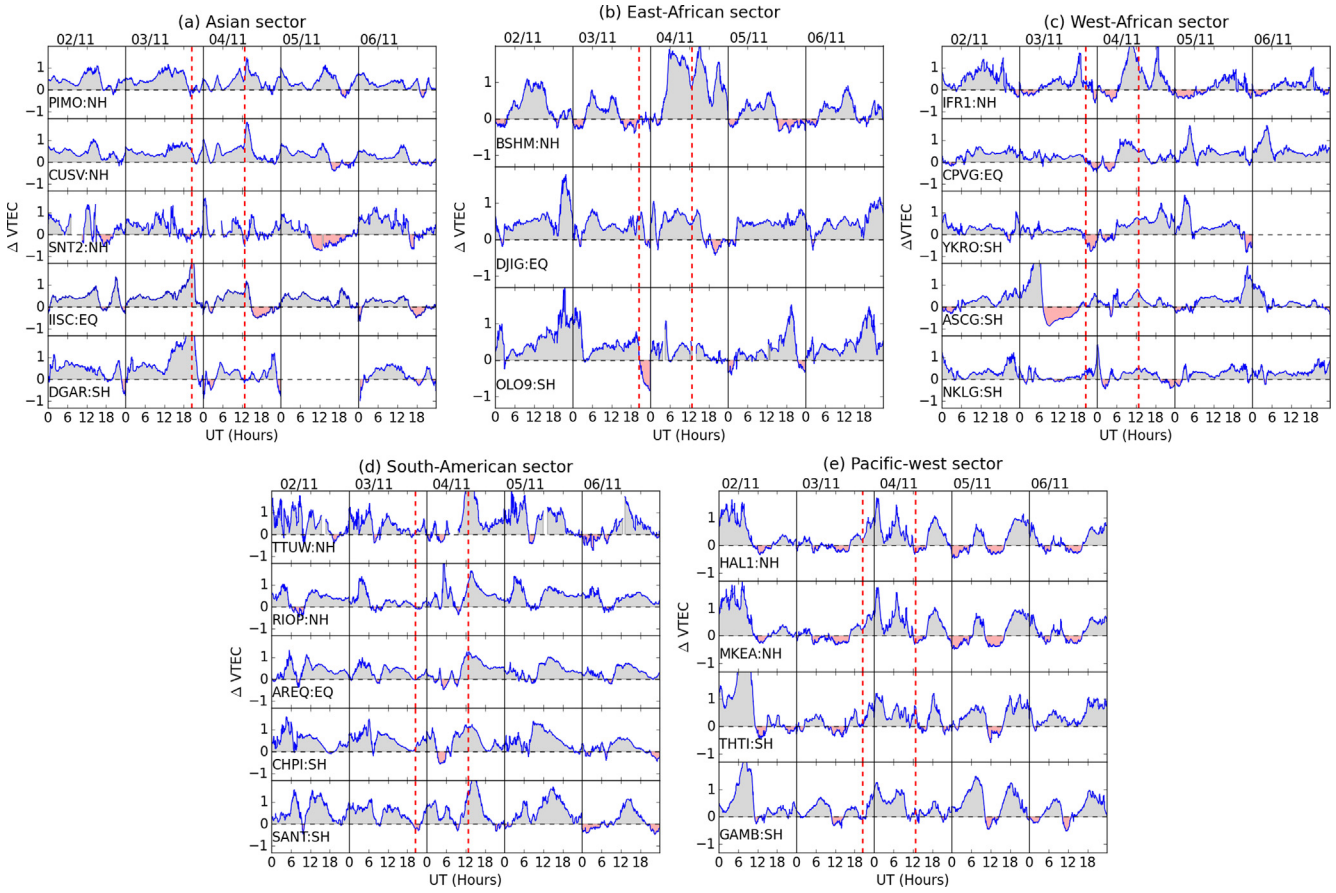


Fig. 4. Variation of ΔVTEC over GPS receiver stations installed in the different longitudinal sectors at low-latitudes during 02–06 November 2021, in panels (a) to (e). The two dotted vertical red lines show the duration of the main phase of the geomagnetic storm. The grey shaded regions represent positive ΔVTEC, while the red shaded regions represent negative ΔVTEC.

2021. Close inspection of the results presented in Fig. 4, show that most of the stations (BSHM, IFR1, RIOP, TTUW, MKEA, HAL1, CUSV, AND PIMO) that encountered highest positive ΔVTEC are located at (or near) the North EIA.

To supplement the ground-based VTEC observations presented in Figs. 3 and 4, the spatial variations of Swarm satellite's LP in situ measurements of N_e and Swarm VTEC measurements were analyzed during the geomagnetic storm period. The Swarm N_e and VTEC variations are presented in Figs. 5 and 6, respectively, for the period 02–06 November, 2021.To examine the spatial variations of Swarm observations, all Swarm equator crossings for each day were considered. From Figs. 5 and 6, there are differences between Swarm A and B in longitudinal distribution of N_e and VTEC. Swarm B shows the lowest values of both N_e and VTEC compared to Swarm A. A similar observation was made by Zakharenkova et al. (2016) and Aol et al. (2020a) who compared the seasonal and longitudinal variation of ionospheric irregularities for Swarm A, B, and C. The differences observed between Swarm A and B can be explained by the altitude and local time separation between the satellites as Swarm B flies at a higher altitude and always crosses the post-sunset sector later than Swarm A. From Figs. 5 and 6, N_e and VTEC enhancements, on 04 November 2021, were more prevalent over the Asian, African, and South American sectors and less prevalent over Pacific-west sector, thereby showing good agreement with ground-based VTEC observations (see Fig. 3). The observed N_e and VTEC enhancement over Asian, African and South American sectors correspond to well developed EIA. Generally, eastward electric field causes vertical uplift of $\vec{E} \times \vec{B}$ drift at the magnetic equator, causing plasma to diffuse along the magnetic field lines to form two peaks of plasma density (crests) at about $\pm 15^{\circ}$ off the magnetic equator and a reduced plasma density at the magnetic equator (trough) in a process similar to a fountain (Appleton, 1946). Ideally, at storm time, the combination of solar photo-ionization and plasma transport enhances EIA plasma densities to values above quiet time levels, creating a positive ionospheric response to geomagnetic storm (Balan et al., 1997). At night, the westward electric field may considerably reduce the TEC and cause a contraction of the EIA. Strong nighttime westward electric fields could lead to total coalition of the EIA structure to form a single strip of plasma density around the equator (Balan et al., 1997). It is also observed from Figs. 5 and 6 that the values of both N_e and VTEC decrease progressively during the

Please cite this article as: S. Aol, V. Habyarimana, P. Mungufeni et al., Ground and Space-based response of the ionosphere during the geomagnetic storm of 02–06 November 2021 over the low-latitudes across different longitudes, Advances in Space Research, https://doi.org/10.1016/j.asr.2023.12.032

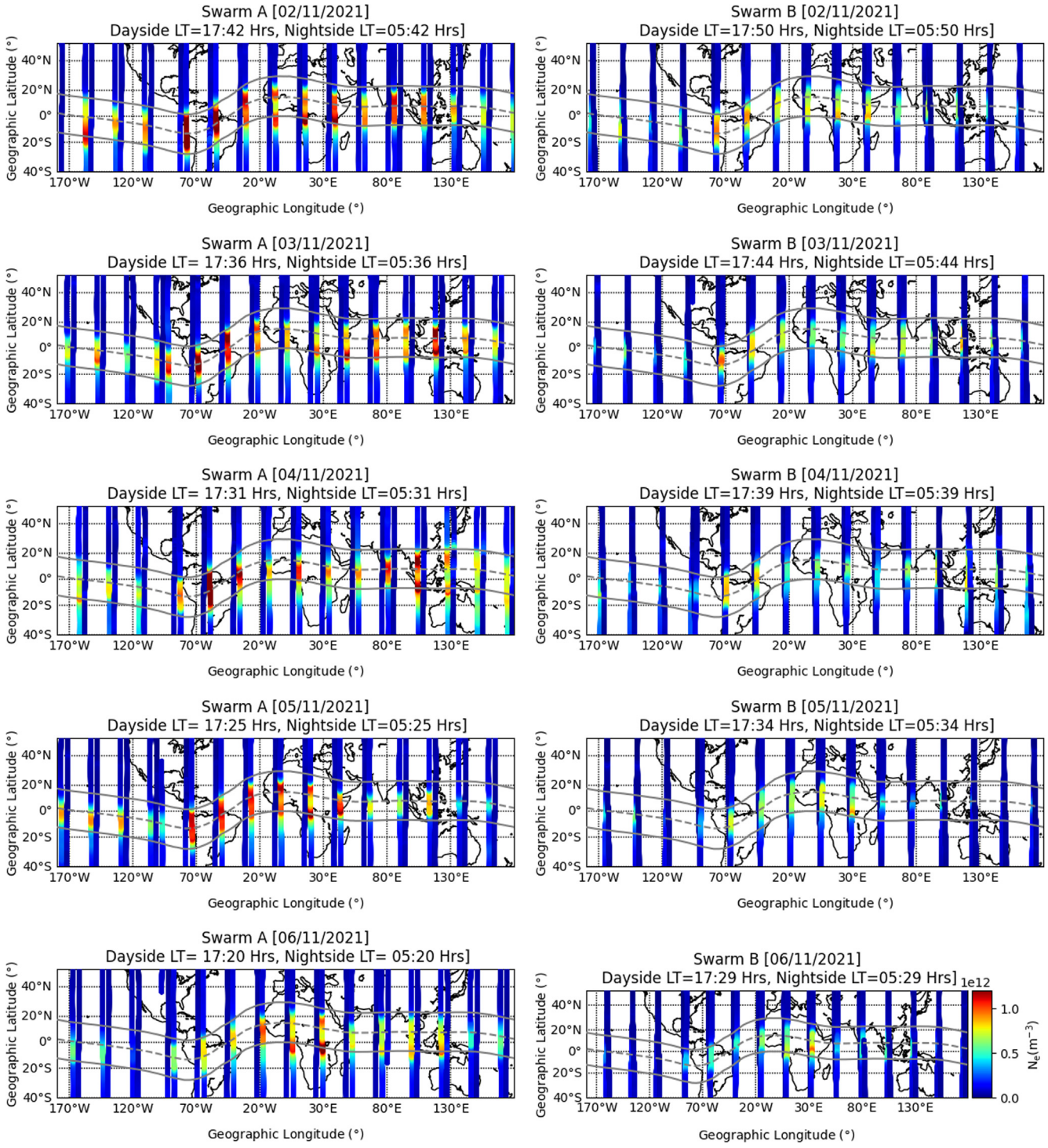


Fig. 5. Spatial variations of Swarm A and B N_e measurements for 02–06 November 2021. The color bar represents In situ N_e.

geomagnetic storm recovery phases on 05–06 November 2021.

Variations of thermospheric composition during geomagnetic storms are closely related to both positive and negative ionospheric storm time responses in the ionosphere (Fuller-Rowell et al., 1994; Rishbeth, 1998; Zhang, 2004; Lei et al., 2010; Cai et al., 2020). To examine the variation of the thermosphere neutral composition during 02 – 06 November 2021, the O/N_2 ratio variation, recorded by Global Ultraviolet Imager (GUVI) instrument onboard the Thermosphere Ionosphere Mesosphere Energetics and Dynamics (TIMED) satellite was used. The variation of O/N_2 ratio is presented in Fig. 7. Generally, the O/N_2 ratio is about 0.4–0.6 at quiet time on 02–06 November 2021. An enhancement in thermospheric O/N_2 over the Asian, African and South American sectors is observed

Please cite this article as: S. Aol, V. Habyarimana, P. Mungufeni et al., Ground and Space-based response of the ionosphere during the geomagnetic storm of 02–06 November 2021 over the low-latitudes across different longitudes, Advances in Space Research, https://doi.org/10.1016/j.asr.2023.12.032

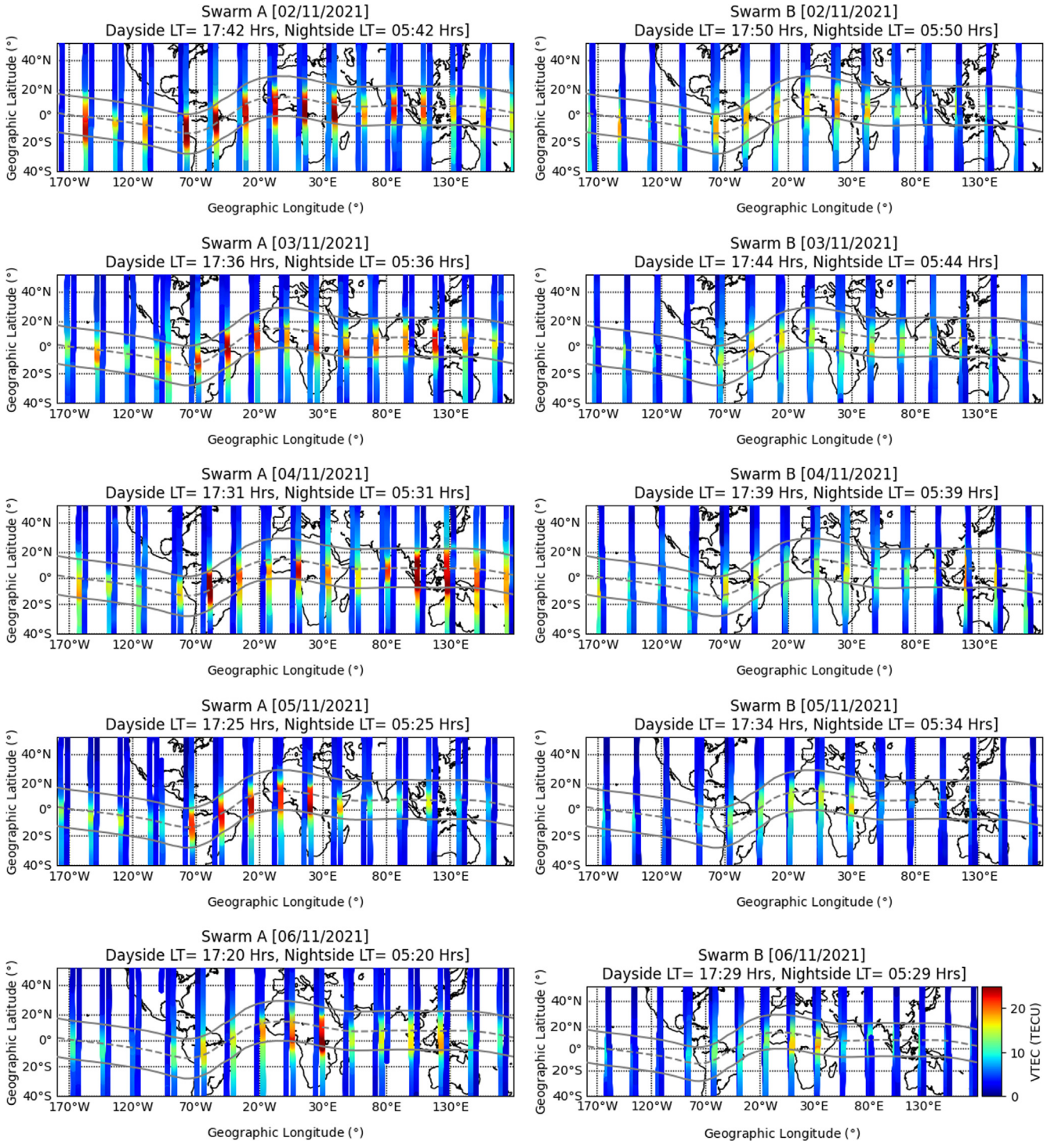


Fig. 6. Spatial variations of Swarm A and B VTEC measurements for November 02–06, 2021. The color bar represents space-based VTEC.

in Fig. 7, on 04 November, 2021. The peaks in O/N_2 occur close to the northern EIA. It was also observed that the O/N_2 ratio returns to its pre-storm profile after the main phase of the geomagnetic storm (i.e., 05–06, November 2021 shown in Fig. 7). The enhancement in O/N_2 ratio on 04 November 2021 may have contributed to an enhancement in VTEC or positive storm effect observed in Fig. 4 (Prölss, 1977; Mayr et al., 1978; Lekshmi et al., 2011; Ratovsky et al., 2018; Lissa et al., 2020). The thermosphere is diffusively separated, with heavier species dominant at lower altitudes and lighter species dominant at higher altitudes (Fuller-Rowell et al., 1996). During geomagnetic storms, the upwelling transports heavier species from the lower thermosphere to higher altitudes and increases the relative abundance of heavier species, while lighter species are left at the lower thermosphere. With

Please cite this article as: S. Aol, V. Habyarimana, P. Mungufeni et al., Ground and Space-based response of the ionosphere during the geomagnetic storm of 02–06 November 2021 over the low-latitudes across different longitudes, Advances in Space Research, https://doi.org/10.1016/j.asr.2023.12.032

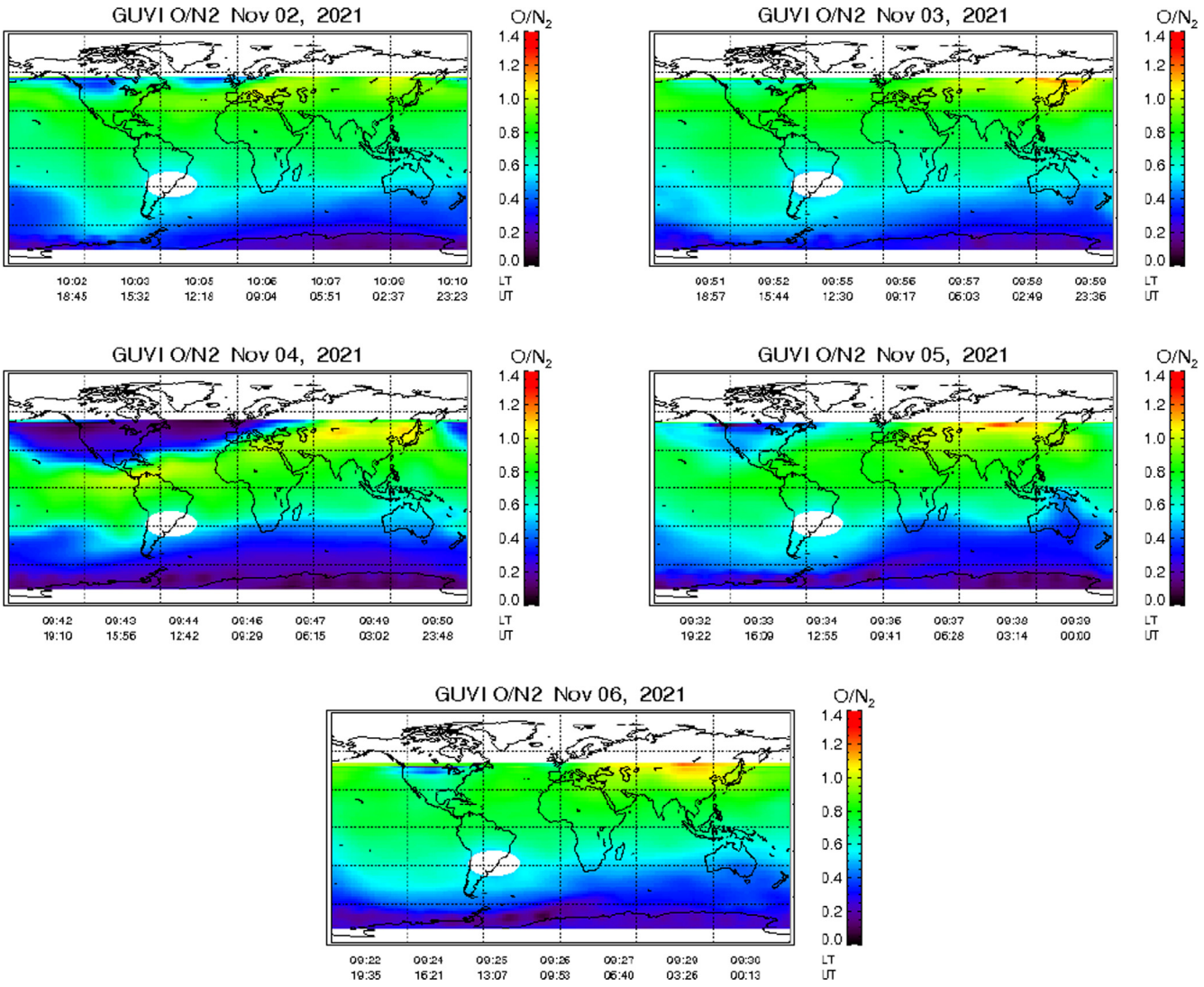


Fig. 7. Variation of O/N_2 ratio from TIMED/GUVI during 02–06 November 2021. The white spaces show missing data.

the lighter species, photo-ionization restores plasma densities at lower altitudes with resultant enhancements in TEC (Tsurutani et al., 2008). During recovery phase of a storm, neutral composition changes play important role in daytime electron density increase (Klimenko et al., 2018). On the other hand, Richmond and Roble (1979) explained how electric currents at the auroral latitudes got enhanced by precipitating particles, field aligned currents, and convection of magnetospheric electric field via Joule heating and momentum transfer by the Ampere force. Joule heating leads to transfer of energy to the neutrals, while Ampere force moves neutral wind by momentum transfer. Both processes drive thermospheric wind (Sharma et al., 2011), which could extend from the high-to-mid-latitude and low-latitude regions (Mazaudier et al., 1985). These winds drag ionization to altitudes where recombination rates are significantly reduced, thereby causing enhancements in TEC. These winds are responsible for global changes in thermospheric composition (Fuller-Rowell et al., 1994) and they are longitudinal dependent.

In addition, to the thermal expansion of the atmosphere, two other large scale physical processes (PPEF and DDEF) affect the dynamics of the ionosphere during magnetic storms and can alter the ionization distribution. Fig. 8 shows the variations of Penetration Electric Field and quiet zonal electric field plus Penetration Electric Field derived from the real-time model of the ionospheric electric fields (Manoj and Maus, 2012) at the five longitudinal sectors ((a) Asian:75°E, (b) East-Africa:30°E, (c) West-Africa:5°W (d) South America:71°W, and (e) Pacific-west:151°W), during 02–06 November, 2021. The Scherliess and Fejer (Scherliess and Fejer, 1999) vertical drift model is used as the quiet zonal electric field, which has positive as eastward. It can be seen from Fig. 8 that the PPEF fluctuations were high during the main phase of the geomagnetic storms in all the longitudinal sectors and damped off during the recovery phase of the storm.There were instances of strong eastward PPEF during day time between about 0600 UT - 1200 UT on 04 November 2021, especially in the Asian, East-African and West-African sectors.

Please cite this article as: S. Aol, V. Habyarimana, P. Mungufeni et al., Ground and Space-based response of the ionosphere during the geomagnetic storm of 02–06 November 2021 over the low-latitudes across different longitudes, Advances in Space Research, https://doi.org/10.1016/j.asr.2023.12.032

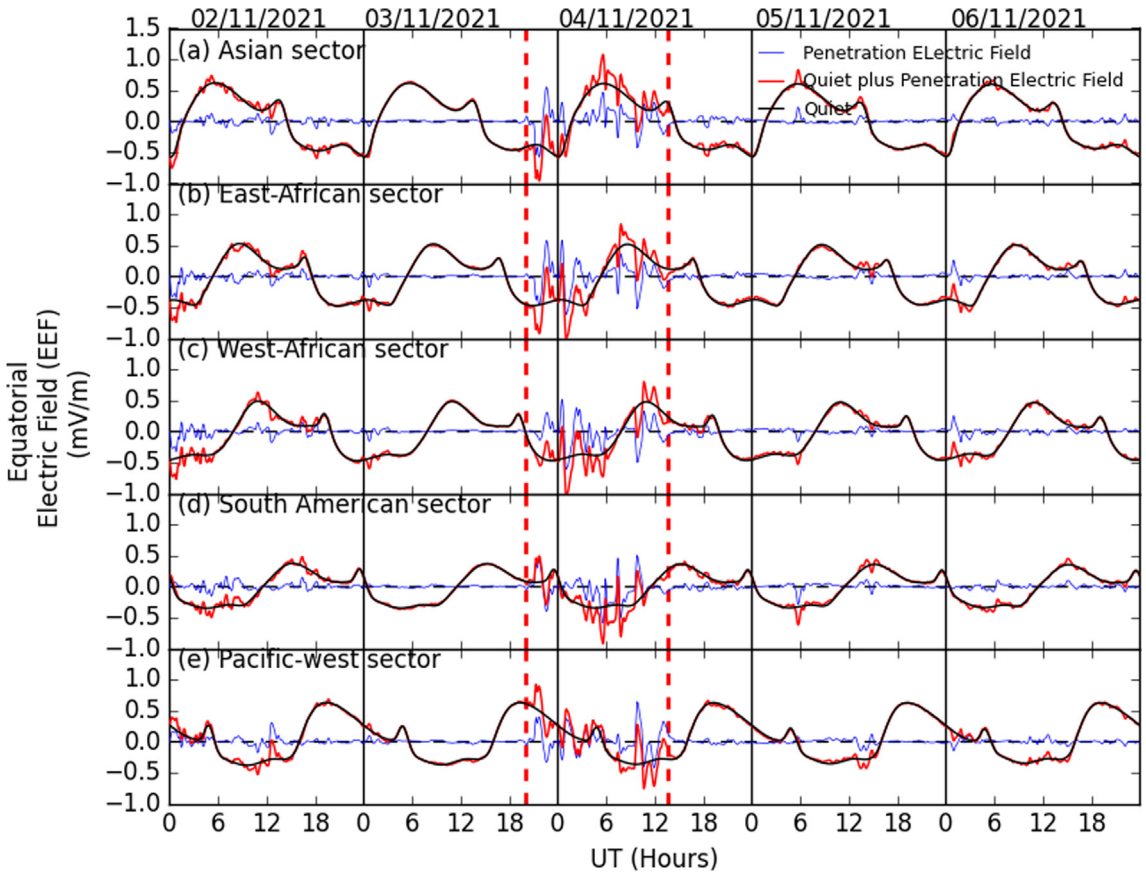


Fig. 8. The variations of Penetration Electric Field and quiet plus penetration electric field (red) derived from the real-time model of the ionospheric electric fields, during 02–06 November, 2021 for the five longitudinal sectors in panels (a)-(e). The blue curve represents the penetration electric field calculated from the IEF-Ey and transfer function (Manoj and Maus, 2012), the black curve represents the quiet background zonal electric field plus the penetration electric field. The two dotted vertical red lines show the duration of the main phase of the ge.omagnetic storm.

Variations in PPEF were highest in the Asian and African sectors. The PPEF occurs during periods of southward IMF Bz, and it can penetrate into the low-latitude for several hours. As is expected, local uplifting of plasma and its redistribution due to the eastward PPEF would have a certain time constant (an hour or so) and has been observed (e.g, Tsurutani, 2004). Therefore, observation of enhancement in VTEC at almost the same time over all the stations with nearly same magnetic latitude points to a common mechanism (i.e, PPEF) for its formation. This result also implies that the day-time PPEF penetrates almost simultaneously over a wide longitude zone.

Fig. 9 shows the storm-time variations of the ionospheric currents at the low latitude observatories in the three major longitudinal sectors i.e., (a) Asian sector: HYB, (b) African sector:TAM, and South America sector:KOU. Each plot shows the four curves corresponding to the variation in the horizontal component of the geomagnetic field (H), the quiet daily variation (S_R), D_{iono}, D_{dyn}, and DP2. Overall, it is observed from Fig. 9 that the variations of all the parameters (i.e, H, D_{iono}, D_{dyn}, and DP2) were highest during the main phase of the geomagnetic storm in all the stations. The oscillations of the four parameters progressively decay during the recovery phase. It is important to mention that at the three magnetometer stations, the signatures of the DP2 parameters maintained rapid oscillations, while the D_{dyn} signatures were characterized with longer-hours. Furthermore, it is observed that the DP2 variations are more in the Asian and African sectors and least in the South American sector. The DP2 results shown in Fig. 9 agree with the PPEF results shown in Fig. 8. On the other hand, D_{dyn} variations are more in the South-American sector and least in the African and Asian sectors. Fathy et al. (2014) and Nava et al. (2016) have also analyzed the D_{dyn} disturbance related to geomagnetic storms and they observed that the diurnal oscillation of D_{dyn} was different from one longitude sector to another. In addition, during the SSC, an increase in the H component is observed in all the stations and this is related to the Chapman-Ferraro current during the compression of the magnetosphere (Chapman and Ferraro, 1931). During the main phase, a decrease in the H component is recorded by the three observatories. The strongest decrease in the H component of the magnetic field is observed at HYB (≈ -200 nT) as compared to the other two stations, i.e., TAM (≈ -100 nT) and KOU (≈ -50 nT). This decreasing trend of the H component is related to the diamagnetic behavior of the ring current. The

Please cite this article as: S. Aol, V. Habyarimana, P. Mungufeni et al., Ground and Space-based response of the ionosphere during the geomagnetic storm of 02–06 November 2021 over the low-latitudes across different longitudes, Advances in Space Research, https://doi.org/10.1016/j.asr.2023.12.032

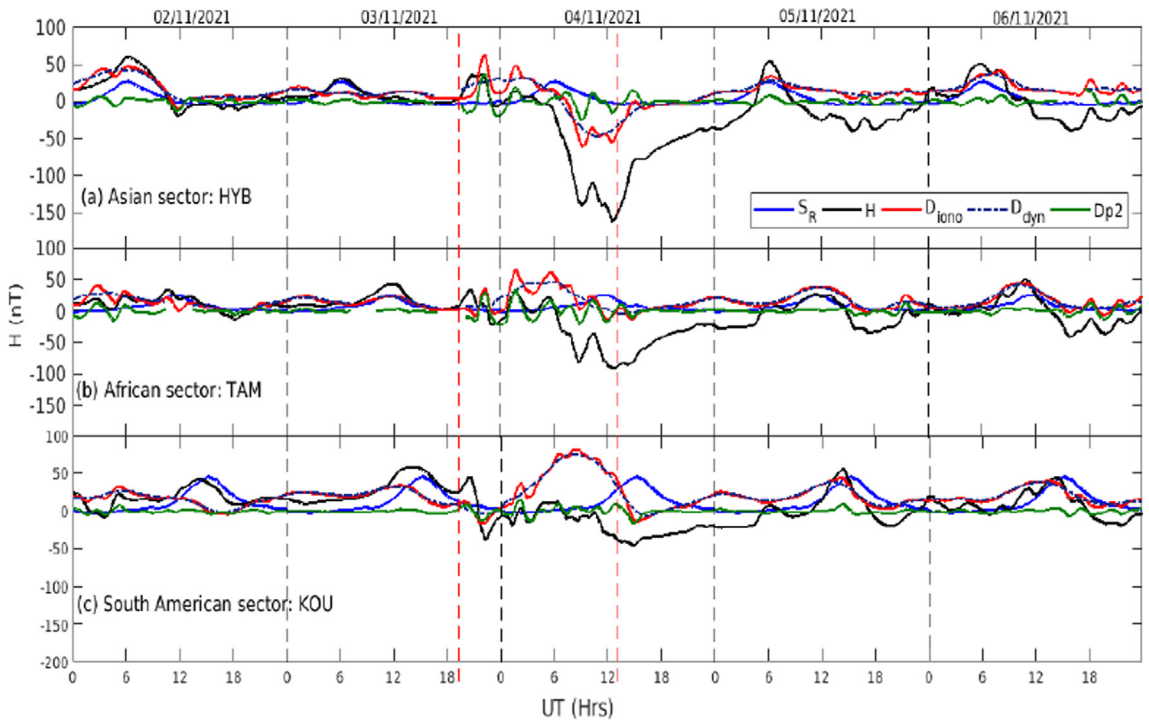


Fig. 9. Magnetic field variations over (a) Asian sector:HYB, (b) African sector:TAM, and South America sector:KOU during the geomagnetic storm period 02–06 November 2021. The two dotted vertical red lines show the duration of the main phase of the geomagnetic storm.

magnetospheric ring current generates the magnetic field opposite to the geomagnetic field. As a result, the H component of the geomagnetic field decreases (Chapman and Ferraro, 1931; Nava et al., 2016). During the recovery phase, the ring current decays and the H component returns to its pre-storm value. Furthermore, during the main phase, the D_{iono} and D_{dyn} mainly had a positive (eastward) orientation at KOU (South American sector, peak≈ 80nT), TAM (African sector, peak≈ 50nT) and HYB (Asian sector, peak≈ 50nT) at different local times. The positive ionospheric storm effect during the main phase at all the longitudinal sectors (see Figs. 3 and 4) may be attributed to equator-ward neutral wind and strong DDEF which was eastward during the main phase of the geomagnetic storm as depicted by D_{dyn} which exceeded DP2 (green curve in Fig. 9) current for the time period between 0000 UT - 0600 UT on 04 November 2021.

4.3. Occurrence of ionospheric irregularities during 02–06 November 2021

Fig. 10 shows the variations of ROTI derived from the GNSS-TEC during the geomagnetic storm period for all the longitudinal sectors. From Figs. 8 and 9, the storm-induced electric fields are more evident on 04 November 2021 and therefore the observed enhancement/inhibition of ionospheric irregularities on 04 November may be attributed to the geomagnetic storm conditions. From Fig. 10, ionospheric irregularities were inhibited on 04 November 2021 in the Asian sector, in all the stations. Ionospheric irregularities were also inhibited in the East-African sector in all the stations on 04 November, 2021. In the West-African sector, the generation of ionospheric irregularities is observed on 02, 03, 05 and 06 November, 2021, but inhibited on 04 November, 2021 in all the stations. In the South American sector, ionospheric irregularities were enhanced for IGS receiver stations RIOP, AREQ, and TTUW (ROTI $>$ 0.3) and this corresponded to the recovery phase of the geomagnetic storm on 04 November 2021. Ionospheric irregularities were inhibited in the Pacific-West sector on 04 November 2021. Bolaji et al. (2019) also observed ionospheric irregularities in some stations in the South American sector for the month of March 2015. This indicates a significant longitudinal variation within the South American sector. To identify space-based ionospheric irregularities, RODI and ROTI were derived from Swarm N_e and VTEC measurements and the results are presented in Fig. 11.It is important to note that the Swarm passes presented in Fig. 11 are dawn passes on 04 November 2021.Information on the UT of Swarm A and B equator crossings is given in Table 2. In

Please cite this article as: S. Aol, V. Habyarimana, P. Mungufeni et al., Ground and Space-based response of the ionosphere during the geomagnetic storm of 02–06 November 2021 over the low-latitudes across different longitudes, Advances in Space Research, https://doi.org/10.1016/j.asr.2023.12.032

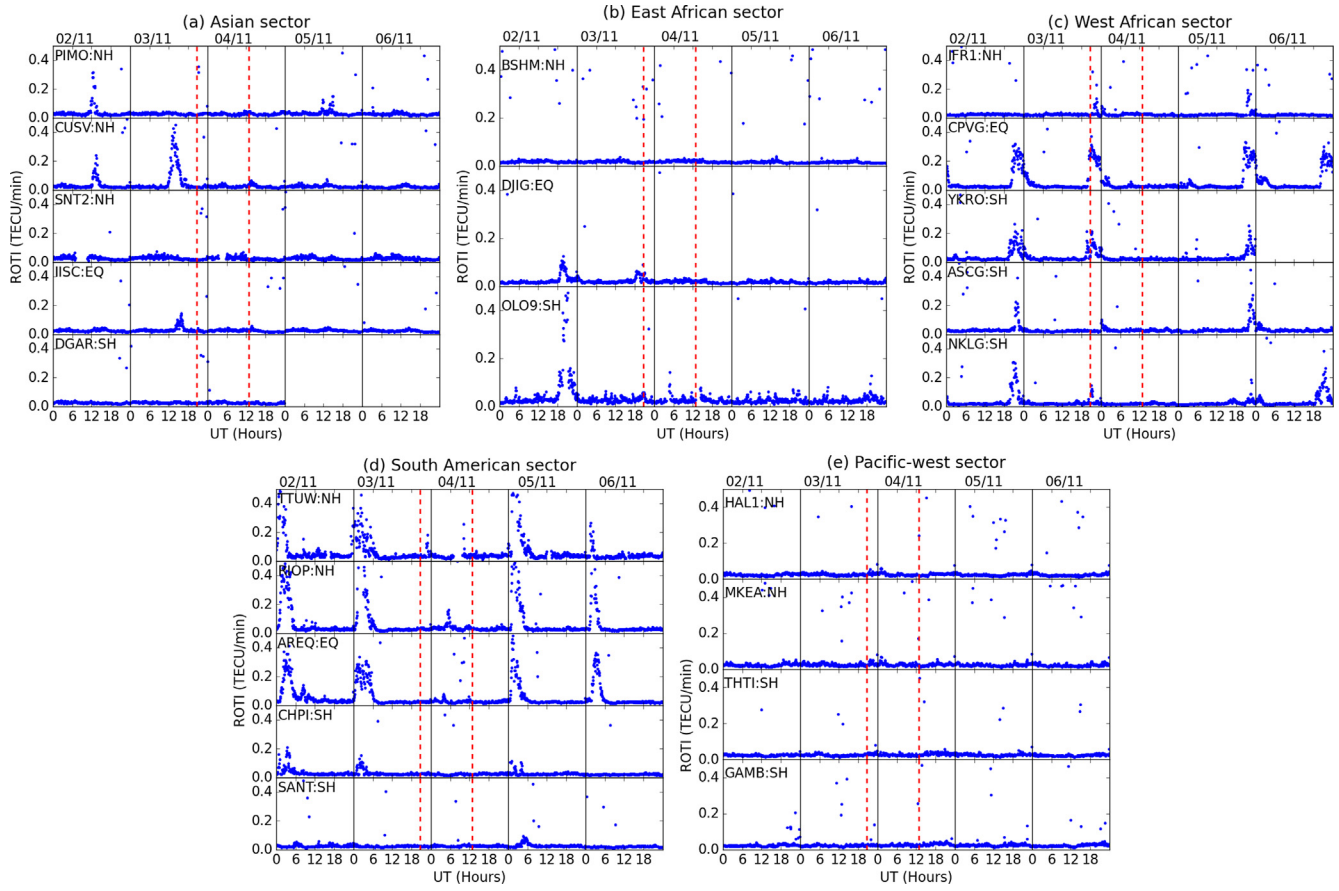


Fig. 10. Variation of ROTI over IGS stations installed in the low latitudes during 02–06 November 2021. Panel (g) shows the variation of SYM-H. The two dotted vertical red lines show the duration of the main phase of the geomagnetic storm.

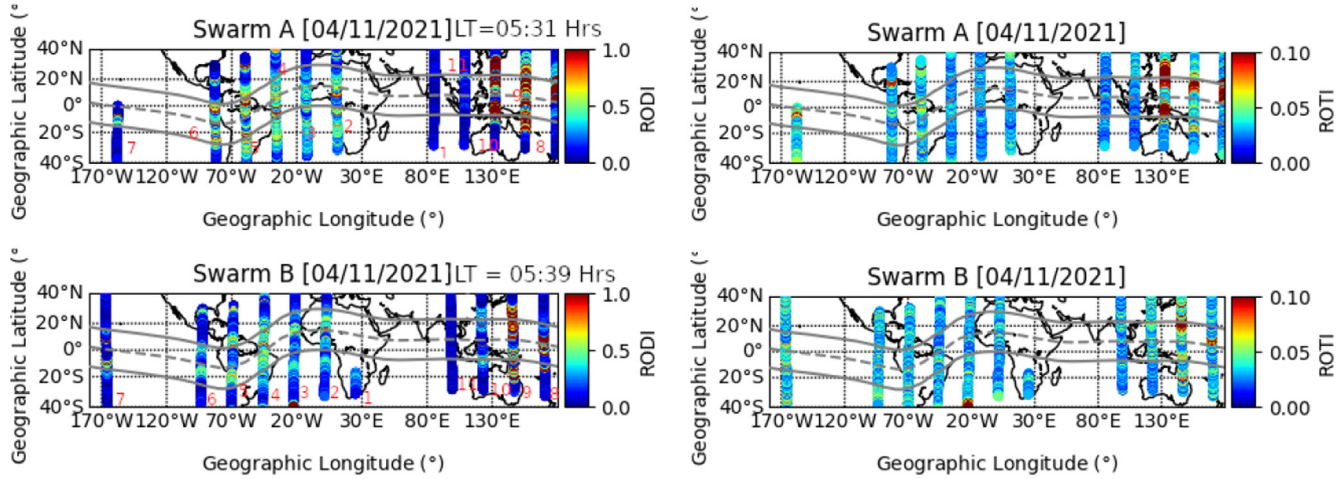


Fig. 11. Ionospheric irregularities as detected by in situ plasma density observations onboard Swarm. The color bars show RODI (first column) and ROTI (second column) distribution for Swarm A and B dawn passes on 04 November 2021. The Swarm passes are identified by serial numbers which are indicated in the left panels..

Table 2, we listed 11 Swarm A/B passes, identified by their serial numbers given in Fig. 11. Fig. 11 shows that only mild occurrences of ionospheric irregularities were recorded in the West-African and South American sector.

Please cite this article as: S. Aol, V. Habyarimana, P. Mungufeni et al., Ground and Space-based response of the ionosphere during the geomagnetic storm of 02–06 November 2021 over the low-latitudes across different longitudes, Advances in Space Research, https://doi.org/10.1016/j.asr.2023.12.032

Table 2
Tracking Times in UT for Swarm A and B at different Passes identified by serial numbers also shown in left panels in Fig. 11.

	Swarm A		Swarm B	
Serial Number	Start UT (HH:MM:SS)	end UT (HH:MM:SS)	Start UT (HH:MM:SS)	End UT (HH:MM:SS)
1	00:16:44	00:35:47	03:57:17	04:17:25
2	04:56:01	05:16:05	05:31:33	05:52:07
3	06:29:29	06:50:38	07:04:26	07:26:19
4	08:03:35	08:26:15	08:36:47	08:59:44
5	09:38:29	10:00:47	10:10:27	10:32:39
6	11:12:39	11:34:03	11:45:21	12:07:01
7	15:49:19	16:10:14	16:33:00	16:54:16
8	18:54:21	19:14:28	18:08:51	18:29:41
9	20:27:41	20:47:13	19:44:20	20:04:32
10	22:01:13	22:20:17	21:19:17	21:38:53
11	23:34:34	23:53:30	22:54:02	23:13:17

Furthermore, Swarm A, and B encountered intense ionospheric irregularities for equator crossings at the Pacific-East sector. From panel (g) of Fig. 10 and the summary provided in Table 1, the onset time of the geomagnetic storm corresponds to early morning hours in Asian sector, post-sunset-pre-midnight hours in the East African and West-African sectors, and pre-noon hours in the Pacific-west sector. From Aarons (1991), the ring current during magnetic storms appears to play a leading role directly or indirectly in establishing the conditions necessary for equatorial F layer irregularity generation or inhibition. The hypothesis advanced is that for a particular ionospheric propagation intersection, the local time when the peak excursion of the ring current occurs (its decay from maximum negative values), affects the equatorial electric field and therefore the height of the F layer. If the maximum ring current energy occurred during the midnight to post-midnight time period, irregularities were generated. If the maximum Dst or SYM-H, the period before recovery set in, occurred in the early afternoon, irregularities were inhibited. If the maximum occurred around sunset or shortly after sunset, then there was no effect on the generation of irregularities that night (Aarons, 1991). Previous studies have used the concept introduced by Aarons (1991) to show that equatorial irregularities occur in the specific longitude sector for which the early evening period corresponds to the time of rapid Dst or SYM-H variation and strongly negative Dst or SYM-H values (e.g, Basu et al., 2001; Martinis, 2005; Dugassa et al., 2019; Bolaji et al., 2019; Aol et al., 2020b; Akala et al., 2021). Furthermore, the generation of irregularities in the South American sector may be associated with eastward DDEF and/or an over-shielding PPEF. After sunset and along the dip equator, the ionospheric plasma is uplifted by the vertical $E \times B$ drift, where the electric field E during the daytime is mapped from the E-region to the F-region (De Rezende et al., 2007). The zonal electric field in the equatorial ionosphere is eastward during the daytime, producing an upward $E \times B/B^2$ drift velocity. Immediately after sunset, this eastward electric field is enhanced due to conductivity gradient at the terminator, a process called the pre-reversal enhancement. The plasma from the F-region at the dip equator is then uplifted to higher altitudes, and at the same time the plasma in the E-regions quickly diminishes due to the decreasing intensity of solar radiation (Kelley, 2009). A sharp upward plasma density gradient is created between the depleted bottom-side ionosphere and the higher density in the topside F-region. Following this, the uplifted plasma begins to descend (or diffuse) along geomagnetic field lines into the low-latitudes by the action of gravity (g) and the pressure gradient (∇p) forces. The density gradients are known to be unstable in the development of plasma density instability mechanisms (Fejer et al., 1999).

5. Conclusions

This study examined the response of the ionosphere at five longitudinal sectors (Asian, East-African, West-African, South-American, and Pacific-west sectors) during the geomagnetic storm for the period 02–06 November, 2021 over the low-latitudes. Both ground-based GPS observations and Space-based Swarm LP and GPS observations were utilised in this study. The ground-based and space-based observations revealed similarities in the patterns of ionospheric response to the geomagnetic storm. The findings are summarized below:

- The low-latitude ionospheric response during the geomagnetic storm showed mostly positive storm effects over all longitudinal sectors. The positive responses of TEC during the storm are attributed to strongly enhanced thermospheric O/N_2. During the geomagnetic storm, vertical upwelling transported heavier species from the lower thermosphere to higher altitudes and increased the relative abundance of heavier species at the higher altitudes, while lighter species were left at the lower thermosphere. With the lighter species, photo-ionization restored plasma densities at lower altitudes resulting to the observed enhancements in TEC. This result validates the thermospheric circulation model by Fuller-Rowell et al. (1994). The PPEF and

DDEF effect may have supported the positive ionospheric storm, and the thermospheric composition variation may have also contributed. A clear hemispherical asymmetry to the advantage of the northern hemisphere at the expense of the southern hemisphere was observed in the distribution of VTEC. This depended on the variation of the thermospheric composition in the two hemispheres.

- The geomagnetic storm during the period 02–06 November 2021, inhibited the occurrence of night-time ionospheric irregularities on 04 November 2021, in almost all longitudinal sectors except for IGS receiver stations RIOP, AREQ and TTUW located in the South American sectors. The local time of the storm's onset and local time of storm's minimum SYM-H are the major determining factors for irregularities generation. Furthermore, the generation of irregularities in the South American sector may be associated with eastward DDEF and/or an over-shielding PPEF. At the equatorial/low-latitude region, during post-sunset hours, PRE-related $\vec{E} \times \vec{B}$ drift creates conducive environment for irregularities generation (Akala et al., 2014). Ionospheric irregularities were only prevalent in the South American sector where the storm's onset and local time of storm's minimum SYM-H correspond to post-sunset hours (21:00–22:00 LT). During the geomagnetic storm, the combined effect of PPEF and PRE intensified post-sunset hours' plasma to support irregularities generation in the South American sectors.

Declaration of Competing Interest

The authors declare that they have no known competing financial interests or personal relationships that could have appeared to influence the work reported in this paper.

Acknowledgments

We acknowledge use of NASA/GSFC's Space Physics Data Facility's OMNIWeb (https://cdaweb.gsfc.nasa.gov) service, and OMNI data. The authors acknowledge the ESA Swarm team for the Swarm mission. The official Swarm website is http://Earth.esa.int/swarm, and the VirES for Swarm data distribution is provided in the website https://vires.services/. In addition, the international GNSS service (IGS) is acknowledged for providing the GPS data. The results presented in this paper rely on data collected at magnetic observatories. We thank the national institutes that support them and INTERMAGNET for promoting high standards of magnetic observatory practice (www.intermagnet.org). The results presented in this paper rely on geomagnetic indices calculated and made available by ISGI Collaborating Institutes from data collected at magnetic observatories. We thank the involved national institutes, the INTERMAGNET network and ISGI (isgi.unistra.fr).

References

Aarons, J., 1991. The role of the ring current in the generation or inhibition of equatorial F-layer irregularities during magnetic storms. Radio Sci. 26 (4), 1131–1149. https://doi.org/10.1029/91rs00473.

De Abreu, A., Fagundes, P., Gende, M., et al., 2014. Investigation of ionospheric response to two moderate geomagnetic storms using GPS–TEC measurements in the south american and african sectors during the ascending phase of solar cycle 24. Adv. Space Res. 53 (9), 1313–1328. https://doi.org/10.1016/j.asr.2014.02.011.

De Abreu, A.J., Fagundes, P.R., Sahai, Y., et al., 2010. Hemispheric asymmetries in the ionospheric response observed in the american sector during an intense geomagnetic storm. J. Geophys. Res.: Space Phys. 115 (A12), A12312. https://doi.org/10.1029/2010ja015661.

Adewale, A.O., Oyeyemi, E.O., Adeloye, A.B., et al., 2011. Responses of equatorial f region to different geomagnetic storms observed by gps in the african sector. J. Geophys. Res.: Space Phys. 116 (A15), A12319. https://doi.org/10.1029/2011JA016998.

Akala, A., Amaeshi, L., Doherty, P., et al., 2014. Characterization of GNSS scintillations over Lagos, Nigeria during the minimum and ascending phases (2009–2011) of solar cycle 24. Adv. Space Res. 53 (1), 37–47. https://doi.org/10.1016/j.asr.2013.09.034.

Akala, A.O., Oyedokun, O.J., Amaechi, P.O., et al., 2021. Solar origins of August 26, 2018 geomagnetic storm: Responses of the interplanetary medium and equatorial/low-latitude ionosphere to the storm. Space Weather 19 (10). https://doi.org/10.1029/2021sw002734.

Akala, A.O., Oyeyemi, E.O., Amaechi, P.O., et al., 2020. Longitudinal responses of the equatorial/low-latitude ionosphere over the oceanic regions to geomagnetic storms of May and September 2017. J. Geophys. Res.: Space Phys. 125 (8). https://doi.org/10.1029/2020ja027963.

Amaechi, P.O., Oyeyemi, E.O., Akala, A.O., 2018. The response of African equatorial/low-latitude ionosphere to 2015 st. Patrick's day geomagnetic storm. Space Weather 16 (6), 601–618. https://doi.org/10.1029/2017sw001751.

Amaechi, P.O., Oyeyemi, E.O., Akala, A.O., et al., 2020. Geomagnetic activity control of irregularities occurrences over the crests of the african EIA. Earth Space Sci. 7 (7). https://doi.org/10.1029/2020ea001183.

Amaechi, P.O., Oyeyemi, E.O., Akala, A.O., et al., 2021. Ground-based GNSS and C/NOFS observations of ionospheric irregularities over Africa: A case study of the 2013 st. Patrick's day geomagnetic storm. Space Weather 19 (2). https://doi.org/10.1029/2020sw002631.

Amory-Mazaudier, C., Bolaji, O.S., Doumbia, V., 2017. On the historical origins of the CEJ, DP2, and Ddyn current systems and their roles in the predictions of ionospheric responses to geomagnetic storms at equatorial latitudes. J. Geophys. Res.: Space Phys. 122 (7), 7827–7833. https://doi.org/10.1002/2017ja024132.

Aol, S., Buchert, S., Jurua, E., 2020a. Traits of sub-kilometre F-region irregularities as seen with the swarm satellites. Ann. Geophys. 38 (1), 243–261. https://doi.org/10.5194/angeo-38-243-2020.

Aol, S., Mungufeni, P., Jurua, E., 2020b. Effects of space weather on the ionosphere: A case study of geomagnetic storms during 17–28 February, 2014. Indian J. Radio Space Phys. (IJRSP) 48 (1–2), 26–37.

Appleton, E.V., 1946. Two anomalies in the ionosphere. Nature 157 (3995). https://doi.org/10.1038/157691a0, 691–691.

Astafyeva, E., Bagiya, M.S., Förster, M., et al., 2020. Unprecedented hemispheric asymmetries during a surprise ionospheric storm: A game of drivers. J. Geophys. Res.: Space Phys. 125 (3). https://doi.org/10.1029/2019ja027261.

Astafyeva, E., Zakharenkova, I., Huba, J.D., et al., 2017. Global ionospheric and thermospheric effects of the June 2015 geomagnetic disturbances: Multi-instrumental observations and modeling. J. Geo-

phys. Res.: Space Phys. 122 (11). https://doi.org/10.1002/2017ja024174.

Astafyeva, E.I., 2009. Dayside ionospheric uplift during strong geomagnetic storms as detected by the CHAMP, SAC-C, TOPEX and Jason-1 satellites. Adv. Space Res. 43 (11), 1749–1756. https://doi.org/10.1016/j.asr.2008.09.036.

Azzouzi, I., Migoya-Orué, Y., Mazaudier, C.A., et al., 2015. Signatures of solar event at middle and low latitudes in the Europe-African sector, during geomagnetic storms, october 2013. Adv. Space Res. 56 (9), 2040–2055. https://doi.org/10.1016/j.asr.2015.06.010.

Balan, N., Bailey, G.J., Abdu, M.A., et al., 1997. Equatorial plasma fountain and its effects over three locations: Evidence for an additional layer, the F3 layer. J. Geophys. Res. 102, 2047–2056. https://doi.org/10.1029/95JA02639.

Banks, P., Araki, T., Clauer, C., et al., 1984. The interplanetary electric field, cleft currents and plasma convection in the polar caps. Planet. Space Sci. 32 (12), 1551–1557. https://doi.org/10.1016/0032-0633(84)90024-2.

Basu, S., Basu, S., Valladares, C.E., et al., 2001. Ionospheric effects of major magnetic storms during the international space weather period of september and october 1999: GPS observations, VHF/UHF scintillations, and in situ density structures at middle and equatorial latitudes. J. Geophys. Res.: Space Phys. 106 (A12), 30389–30413. https://doi.org/10.1029/2001ja001116.

Basu, S., Groves, K., Quinn, J., et al., 1999. A comparison of TEC fluctuations and scintillations at ascension island. J. Atmos. Solar Terr. Phys. 61 (16), 1219–1226. https://doi.org/10.1016/s1364-6826(99)00052-8.

Blagoveshchensky, D., Pirog, O., Polekh, N., et al., 2003. Mid-latitude effects of the May 15, 1997 magnetic storm. J. Atmos. Solar Terr. Phys. 65 (2), 203–210. https://doi.org/10.1016/s1364-6826(02)00227-4.

Blanc, M., Richmond, A., 1980. The ionospheric disturbance dynamo. J. Geophys. Res. 85 (A4), 1669. https://doi.org/10.1029/ja085ia04p01669.

Bolaji, O.S., Adebiyi, S.J., Fashae, J.B., 2019. Characterization of ionospheric irregularities at different longitudes during quiet and disturbed geomagnetic conditions. J. Atmos. Solar Terr. Phys. 182, 93–100. https://doi.org/10.1016/j.jastp.2018.11.007.

Borries, C., Berdermann, J., Jakowski, N., et al., 2015. Ionospheric storms-a challenge for empirical forecast of the total electron content. J. Geophys. Res.: Space Phys. 120 (4), 3175–3186. https://doi.org/10.1002/2015ja020988.

Buchert, S., Zangerl, F., Sust, M., et al., 2015. SWARM observations of equatorial electron densities and topside GPS track losses. Geophys. Res. Lett. 42 (7), 2088–2092. https://doi.org/10.1002/2015gl063121.

Buonsanto, M., 1999. Ionospheric storms-a review. Space Sci. Rev. 88 (3/4), 563–601. https://doi.org/10.1023/a:1005107532631.

Cai, X., Burns, A.G., Wang, W., et al., 2020. The two-dimensional evolution of thermospheric O/N2 response to weak geomagnetic activity during solar-minimum observed by GOLD. Geophys. Res. Lett. 47 (18). https://doi.org/10.1029/2020gl088838.

Chapman, S., Ferraro, V.C.A., 1931. A new theory of magnetic storms. J. Geophys. Res. 36 (3), 171. https://doi.org/10.1029/te036i003p00171.

Cherniak, I., Zakharenkova, I., 2022. Development of the storm-induced ionospheric irregularities at equatorial and middle latitudes during the 25–26 August 2018 geomagnetic storm. Space Weather 20 (2). https://doi.org/10.1029/2021sw002891.

Dashora, N., Sharma, S., Dabas, R.S., et al., 2009. Large enhancements in low latitude total electron content during 15 May 2005 geomagnetic storm in indian zone. Ann. Geophys. 27 (5), 1803–1820. https://doi.org/10.5194/angeo-27-1803-2009.

Dugassa, T., Habarulema, J.B., Nigussie, M., 2019. Longitudinal variability of occurrence of ionospheric irregularities over the American, African and Indian regions during geomagnetic storms. Adv. Space Res. 63 (8), 2609–2622. https://doi.org/10.1016/j.asr.2019.01.001.

Fathy, I., Amory-Mazaudier, C., Fathy, A., et al., 2014. Ionospheric disturbance dynamo associated to a coronal hole: Case study of 5–10 April 2010. J. Geophys. Res.: Space Phys. 119 (5), 4120–4133. https://doi.org/10.1002/2013ja019510.

Fejer, B., 1991. Low latitude electrodynamic plasma drifts: A review. J. Atmos. Terr. Phys. 53 (8), 677–693.

Fejer, B.G., Jensen, J.W., Su, S.-Y., 2008. Seasonal and longitudinal dependence of equatorial disturbance vertical plasma drifts. Geophys. Res. Lett. 35 (20). https://doi.org/10.1029/2008gl035584.

Fejer, B.G., Scherliess, L., 1995. Time dependent response of equatorial ionospheric electric fields to magnetospheric disturbances. Geophys. Res. Lett. 22 (7), 851–854. https://doi.org/10.1029/95gl00390.

Fejer, B.G., Scherliess, L., De Paula, E.R., 1999. Effects of the vertical plasma drift velocity on the generation and evolution of equatorial spread F. J. Geophys. Res.: Space Phys. 104 (A9), 19859–19869. https://doi.org/10.1029/1999ja900271.

Friis-Christensen, E., Lühr, H., Hulot, G., 2006. Swarm: A constellation to study the earth's magnetic field. Earth, Planets and Space 58 (4), 351–358. https://doi.org/10.1186/bf03351933.

Fuller-Rowell, T.J., Codrescu, M.V., Moffett, R.J., et al., 1994. Response of the thermosphere and ionosphere to geomagnetic storms. J. Geophys. Res. 99 (A3), 3893. https://doi.org/10.1029/93ja02015.

Fuller-Rowell, T.J., Codrescu, M.V., Rishbeth, H., et al., 1996. On the seasonal response of the thermosphere and ionosphere to geomagnetic storms. J. Geophys. Res.: Space Phys. 101 (A2), 2343–2353. https://doi.org/10.1029/95ja01614.

Gonzalez, W., de Gonzalez, A.C., Sobral, J., et al., 2001. Solar and interplanetary causes of very intense geomagnetic storms. J. Atmos. Solar Terr. Phys. 63 (5), 403–412. https://doi.org/10.1016/s1364-6826(00)00168-1.

Gonzalez, W.D., Joselyn, J.A., Kamide, Y., et al., 1994. What is a geomagnetic storm? J. Geophys. Res. 99 (A4), 5771. https://doi.org/10.1029/93ja02867.

Gonzalez, W.D., Tsurutani, B.T., 1987. Criteria of interplanetary parameters causing intense magnetic storms (dst < -100 nT). Planet. Space Sci. 35 (9), 1101–1109. https://doi.org/10.1016/0032-0633(87)90015-8.

Habarulema, J.B., McKinnell, L.-A., Burešová, D., et al., 2013. A comparative study of TEC response for the African equatorial and mid-latitudes during storm conditions. J. Atmos. Solar Terr. Phys. 102, 105–114. https://doi.org/10.1016/j.jastp.2013.05.008.

Huang, C.-S., Foster, J.C., Kelley, M.C., 2005. Long-duration penetration of the interplanetary electric field to the low-latitude ionosphere during the main phase of magnetic storms. J. Geophys. Res. 110 (A11). https://doi.org/10.1029/2005ja011202.

Huang, C.-S., Yumoto, K., 2006. Quantification and hemispheric asymmetry of low-latitude geomagnetic disturbances caused by solar wind pressure enhancements. J. Geophys. Res. 111 (A9). https://doi.org/10.1029/2006ja011831.

Imtiaz, N., Ali, O.H., Rizvi, H., 2021. Impact of the intense geomagnetic storm of August 2018 on the equatorial and low latitude ionosphere. Astrophys. Space Sci. 366 (11). https://doi.org/10.1007/s10509-021-04009-2.

Kelley, M.C., 2009. The Earth's ionosphere: Plasma physics and electrodynamics. Academic press.

Kikuchi, T., Hashimoto, K.K., Nozaki, K., 2008. Penetration of magnetospheric electric fields to the equator during a geomagnetic storm. J. Geophys. Res.: Space Phys. 113 (A6), A06214. https://doi.org/10.1029/2007ja012628.

Kikuchi, T., Lühr, H., Kitamura, T., et al., 1996. Direct penetration of the polar electric?eld to the equator during a DP2 event as detected by the auroral and equatorial magnetometer chains and the eiscat radar. J. Geophys. Res.: Space Phys. 101 (A8), 17161–17173. https://doi.org/10.1029/96ja01299.

Kil, H., Heelis, R.A., 1998. Global distribution of density irregularities in the equatorial ionosphere. J. Geophys. Res.: Space Phys. 103 (A1), 407–417. https://doi.org/10.1029/97ja02698.

Klimenko, M., Klimenko, V., 2012. Disturbance dynamo, prompt penetration electric field and overshielding in the earth's ionosphere during geomagnetic storm. J. Atmos. Solar Terr. Phys. 90–91, 146–155. https://doi.org/10.1016/j.jastp.2012.02.018.

Please cite this article as: S. Aol, V. Habyarimana, P. Mungufeni et al., Ground and Space-based response of the ionosphere during the geomagnetic storm of 02–06 November 2021 over the low-latitudes across different longitudes, Advances in Space Research, https://doi.org/10.1016/j.asr.2023.12.032

Klimenko, M., Klimenko, V., Despirak, I., et al., 2018. Disturbances of the thermosphere-ionosphere-plasmasphere system and auroral electrojet at 30°E longitude during the st. Patrick's day geomagnetic storm on 17–23 March 2015. J. Atmos. Solar Terr. Phys. 180, 78–92. https://doi.org/10.1016/j.jastp.2017.12.017.

Kumar, S., Chandra, H., Sharma, S., 2005. Geomagnetic storms and their ionospheric effects observed at the equatorial anomaly crest in the indian region. J. Atmos. Solar Terr. Phys. 67, 581–594. https://doi.org/10.1016/j.jastp.2004.12.003.

Laboratories, S.E.S. (2017). Swarm L2 TEC product description, (4.0). URL: https://earth.esa.int/eogateway/documents/20142/37627/.

Le Huy, M., Amory-Mazaudier, C., 2005. Magnetic signature of the ionospheric disturbance dynamo at equatorial latitudes: "Ddyn". J. Geophys. Res.: Space Phys. 110 (A10), A10301, URL: https://agupubs.onlinelibrary.wiley.com/doi/abs/10.1029/2004JA010578.

Lei, J., Thayer, J.P., Burns, A.G., et al., 2010. Wind and temperature effects on thermosphere mass density response to the November 2004 geomagnetic storm. J. Geophys. Res.: Space Phys. 115 (A5), A5303. https://doi.org/10.1029/2009ja014754.

Lekshmi, D.V., Balan, N., Ram, S.T., et al., 2011. Statistics of geomagnetic storms and ionospheric storms at low and mid latitudes in two solar cycles. J. Geophys. Res.: Space Phys. 116 (A11). https://doi.org/10.1029/2011ja017042, n/a–n/a.

Lepping, R.P., Burlaga, L.F., Tsurutani, B.T., et al., 1991. The interaction of a very large interplanetary magnetic cloud with the magnetosphere and with cosmic rays. J. Geophys. Res. 96 (A6), 9425. https://doi.org/10.1029/91ja00670.

Lissa, D., Srinivasu, V., Prasad, D., et al., 2020. Ionospheric response to the 26 august 2018 geomagnetic storm using GPS-TEC observations along 80° e and 120° e longitudes in the asian sector. Adv. Space Res. 66 (6), 1427–1440. https://doi.org/10.1016/j.asr.2020.05.025.

Manoj, C., Maus, S., 2012. A real-time forecast service for the ionospheric equatorial zonal electric field. Space Weather 10 (9). https://doi.org/10.1029/2012sw000825, n/a–n/a.

Mansilla, G.A., Zossi, M.M., 2022. Ionospheric response to the 26 august 2018 geomagnetic storm along 280° e and 316° e in the south american sector. Adv. Space Res. 69 (1), 48–58, URL: https://www.sciencedirect.com/science/article/pii/S0273117721006360.

Martinis, C.R., 2005. Toward a synthesis of equatorial spread F onset and suppression during geomagnetic storms. J. Geophys. Res. 110 (A7). https://doi.org/10.1029/2003ja010362.

Mayr, H.G., Harris, I., Spencer, N.W., 1978. Some properties of upper atmosphere dynamics. Rev. Geophys. 16 (4), 539–565. https://doi.org/10.1029/rg016i004p00539.

Mazaudier, C., Bernard, R., Venkateswaran, S.V., 1985. Correction to Saint-Santin Radar observations of lower thermospheric storms. J. Geophys. Res. 90 (A7), 6685. https://doi.org/10.1029/ja090ia07p06685.

Nava, B., Rodríguez-Zuluaga, J., Alazo-Cuartas, K., et al., 2016. Middle- and low-latitude ionosphere response to 2015 st. Patrick's day geomagnetic storm. J. Geophys. Res.: Space Phys. 121 (4), 3421–3438. https://doi.org/10.1002/2015ja022299.

Ngwira, C.M., Habarulema, J.-B., Astafyeva, E., et al., 2019. Dynamic response of ionospheric plasma density to the geomagnetic storm of 22–23 June 2015. J. Geophys. Res.: Space Phys. 124 (8), 7123–7139. https://doi.org/10.1029/2018ja026172.

Nishida, A., 1968. Geomagnetic DP2 fluctuations and associated magnetospheric phenomena. J. Geophys. Res. 73 (5), 1795–1803. https://doi.org/10.1029/ja073i005p01795.

Noja, M., Stolle, C., Park, J., et al., 2013. Long-term analysis of ionospheric polar patches based on CHAMP TEC data. Radio Science 48 (3), 289–301. https://doi.org/10.1002/rds.20033.

Oladipo, O.A., Adeniyi, J.O., Olawepo, A.O., et al., 2014. Large-scale ionospheric irregularities occurrence at ilorin, nigeria. Space Weather 12 (5), 300–305. https://doi.org/10.1002/2013sw000991.

Oljira, A., 2023. A study of solar flares and geomagnetic storms impact on total electron content over high-latitude region during july- november 2021: The case of tromso station. Adv. Space Res. https://doi.org/10.1016/j.asr.2023.06.051, URL: https://doi.org/10.1016/j.asr.2023.06.051.

Palma, F., Sotgiu, A., Parmentier, A., et al., 2021. The august 2018 geomagnetic storm observed by the high-energy particle detector on board the CSES-01 satellite. Applied Sciences 11 (12), 5680. https://doi.org/10.3390/app11125680.

Papitashvili, N.E., & King, J.H. (2020). OMNI 1-min data set. URL: https://hpde.io/NASA/NumericalData/OMNI/HighResolutionObservations/Version1/PT1M.

Pi, X., Mannucci, A.J., Lindqwister, U.J., et al., 1997. Monitoring of global ionospheric irregularities using the worldwide GPS network. Geophys. Res. Lett. 24 (18), 2283–2286. https://doi.org/10.1029/97gl02273.

Piersanti, M., Michelis, P.D., Moro, D.D., et al., 2020. From the sun to earth: effects of the 25 august 2018 geomagnetic storm. Ann. Geophys. 38 (3), 703–724. https://doi.org/10.5194/angeo-38-703-2020.

Prölss, G.W., 1977. Seasonal variations of atmospheric-ionospheric disturbances. J. Geophys. Res. 82 (10), 1635–1640. https://doi.org/10.1029/ja082i010p01635.

Prölss, G.W., 1995. Ionospheric F-region storms, handbook of atmospheric electrodynamics vol. 2.

Ratovsky, K.G., Klimenko, M.V., Klimenko, V.V., et al., 2018. Aftereffects of geomagnetic storms: statistical analysis and theoretical explanation. Solar-Terrestrial Physics 4 (4), 26–32. https://doi.org/10.12737/stp-44201804.

Regi, M., Perrone, L., Corpo, A.D., et al., 2022. Space weather effects observed in the northern hemisphere during november 2021 geomagnetic storm: The impacts on plasmasphere, ionosphere and thermosphere systems. Remote Sensing 14 (22), 5765. https://doi.org/10.3390/rs14225765.

De Rezende, L.F.C., De Paula, E.R., Batista, I.S., et al., 2007. Study of ionospheric irregularities during intense magnetic storms. Revista Brasileira de Geofísica 25, 151–158. https://doi.org/10.1590/s0102-261x2007000600017.

Richmond, A., Roble, R., 1979. Dynamic effects of aurora-generated gravity waves on the mid-latitude ionosphere. Journal of Atmospheric and terrestrial Physics 41 (7–8), 841–852.

Richmond, A., Roble, R., 1997. Electrodynamic coupling effects in the thermosphere/ionosphere system. Adv. Space Res. 20 (6), 1115–1124. https://doi.org/10.1016/S0273-1177(97)00754-0.

Rishbeth, H. (1989). F-region storms and thermospheric circulation. In P. E. Sandholt, & A. Egeland (Eds.), Electromagnetic Coupling in the Polar Clefts and Caps (p. 393).

Rishbeth, H., 1998. How the thermospheric circulation affects the ionospheric F2-layer. J. Atmos. Solar Terr. Phys. 60 (14), 1385–1402. https://doi.org/10.1016/s1364-6826(98)00062-5.

Rukundo, W., 2023. The ionospheric dynamics of the african sector responding to a severe geomagnetic storm; the storm of 3–5 november 2021. Space Weather 21 (3). https://doi.org/10.1029/2022sw003219.

Sahai, Y., Fagundes, P.R., Becker-Guedes, F., et al., 2005. Effects of the major geomagnetic storms of october 2003 on the equatorial and low-latitude F region in two longitudinal sectors. J. Geophys. Res. 110 (A12). https://doi.org/10.1029/2004ja010999.

Scherliess, L., Fejer, B.G., 1999. Radar and satellite global equatorial f region vertical drift model. J. Geophys. Res.: Space Phys. 104 (A4), 6829–6842. https://doi.org/10.1029/1999ja900025.

Schunk, R., Nagy, A., 2009. Ionospheres: physics, plasma physics, and chemistry. Cambridge University Press. https://doi.org/10.1017/cbo9780511635342.

Seemala, G.K., Valladares, C.E., 2011. Statistics of total electron content depletions observed over the South American continent for the year 2008. Radio Science 46, 5019. https://doi.org/10.1029/2011RS004722.

Sharma, S., Galav, P., Dashora, N., et al., 2011. Longitudinal study of the ionospheric response to the geomagnetic storm of 15 May 2005 and manifestation of TADs. Ann. Geophys. 29 (6), 1063–1070. https://doi.org/10.5194/angeo-29-1063-2011.

Shimeis, A., Fathy, I., Amory-Mazaudier, C., et al., 2012. Signature of the coronal hole near the north crest equatorial anomaly over Egypt

Please cite this article as: S. Aol, V. Habyarimana, P. Mungufeni et al., Ground and Space-based response of the ionosphere during the geomagnetic storm of 02–06 November 2021 over the low-latitudes across different longitudes, Advances in Space Research, https://doi.org/10.1016/j.asr.2023.12.032

during the strong geomagnetic storm 5 April 2010. J. Geophys. Res.: Space Phys. 117 (A7), A07309. https://doi.org/10.1029/2012ja017753.

Smith, A.R.A., Pačes, M., Swarm, D., 2022. Python tools for ESA's swarm mission: VirES for swarm and surrounding ecosystem. Frontiers in Astronomy and Space Sciences 9. https://doi.org/10.3389/fspas.2022.1002697.

Spogli, L., Sabbagh, D., Regi, M., et al., 2021. Ionospheric response over brazil to the august 2018 geomagnetic storm as probed by CSES-01 and swarm satellites and by local ground-based observations. J. Geophys. Res.: Space Phys. 126 (2). https://doi.org/10.1029/2020ja028368.

Srinivasu, V.K.D., Prasad, D.S.V.V.D., Niranjan, K., et al., 2019. L-band scintillation and TEC variations on st. patrick's day storm of 17 March 2015 over indian longitudes using GPS and GLONASS observations. J. Earth Syst. Sci. 128 (3). https://doi.org/10.1007/s12040-019-1097-6.

Tang, J., Gao, X., Yang, D., et al., 2022. Local persistent ionospheric positive responses to the geomagnetic storm in august 2018 using BDS-GEO satellites over low-latitude regions in eastern hemisphere. Remote Sensing 14 (9), 2272. https://doi.org/10.3390/rs14092272.

Tsurutani, B., 2004. Global dayside ionospheric uplift and enhancement associated with interplanetary electric fields. J. Geophys. Res. 109 (A8). https://doi.org/10.1029/2003ja010342.

Tsurutani, B.T., Verkhoglyadova, O.P., Mannucci, A.J., et al., 2008. Prompt penetration electric fields (PPEFs) and their ionospheric effects during the great magnetic storm of 30–31 October 2003. J. Geophys. Res.: Space Phys. 113 (A5), A05311. https://doi.org/10.1029/2007ja012879.

Vankadara, S., R.K.and Panda, Amory-Mazaudier, C., Fleury, R. et al. (2022). Signatures of equatorial plasma bubbles and ionospheric scintillations from magnetometer and GNSS observations in the indian longitudes during the space weather events of early september 2017. Remote Sensing, 14(3), 652. URL: https://doi.org/10.3390/rs14030652.

Wan, X., Zhong, J., Zhang, S.-R., et al., 2022. Disturbance neutral winds effects on the ionospheric strip-like bulge at lower-middle latitudes. J. Geophys. Res.: Space Phys. 127 (8). https://doi.org/10.1029/2022ja030541.

Wang, X., Jin, Y., Meng, X., et al., 2022. Atmospheric density response to a severe magnetic storm detected by the 520 km altitude spherical satellite. Atmosphere 13 (11), 1891. https://doi.org/10.3390/atmos13111891.

Woodman, R.F., La-Hoz, C., 1976. Radar observations of F region equatorial irregularities. J. Geophys. Res. 81 (31), 5447–5466. https://doi.org/10.1029/ja081i031p05447.

Younas, W., Amory-Mazaudier, C., Khan, M., et al., 2020. Ionospheric and magnetic signatures of a space weather event on 25–29 august 2018: CME and HSSWs. J. Geophys. Res.: Space Phys. 125 (8). https://doi.org/10.1029/2020ja027981.

Zakharenkova, I., Astafyeva, E., 2015. Topside ionospheric irregularities as seen from multisatellite observations. J. Geophys. Res.: Space Phys. 120 (1), 807–824, URL: https://agupubs.onlinelibrary.wiley.com/doi/abs/10.1002/2014JA020330.

Zakharenkova, I., Astafyeva, E., Cherniak, I., 2016. GPS and in situ Swarm observations of the equatorial plasma density irregularities in the topside ionosphere. Earth, Planets and Space 68 (1). https://doi.org/10.1186/s40623-016-0490-5.

Zakharenkova, I., Cherniak, I., 2018. Underutilized spaceborne GPS observations for space weather monitoring. Space Weather 16 (4), 345–362. https://doi.org/10.1002/2017sw001756.

Zakharenkova, I., Cherniak, I., Krankowski, A., 2019. Features of storm-induced ionospheric irregularities from ground-based and spaceborne GPS observations during the 2015 st. Patrick's day storm. J. Geophys. Res.: Space Phys. 124 (12), 10728–10748. https://doi.org/10.1029/2019ja026782.

Zhai, C., Tang, S., Peng, W., et al., 2022. Driver of the positive ionospheric storm over the South American sector during 4 November 2021 geomagnetic storm. Remote Sens. 15 (1), 111. https://doi.org/10.3390/rs15010111.

Zhang, Y., 2004. O/N2 changes during 1–4 October 2002 storms: IMAGE SI-13 and TIMED/GUVI observations. J. Geophys. Res. 109 (A10). https://doi.org/10.1029/2004ja010441.

Please cite this article as: S. Aol, V. Habyarimana, P. Mungufeni et al., Ground and Space-based response of the ionosphere during the geomagnetic storm of 02–06 November 2021 over the low-latitudes across different longitudes, Advances in Space Research, https://doi.org/10.1016/j.asr.2023.12.032